Supported and Coordinated Single Metal Site Electrocatalysts

Qiurong Shi[1,†], Sooyeon Hwang[2,†], Haipeng Yang[3,†], Fatma Ismail[4], Dong Su[2]*, Drew Higgins[4,]* and Gang Wu[1,]*

[1], Department of Chemical and Biological Engineering, University at Buffalo, The State University of New York, Buffalo, New York 14260, United States

[2], Center for Functional Nanomaterials, Brookhaven National Laboratory, Upton, New York 11973, United States

[3], College of Materials Science and Engineering, Shenzhen University, Shenzhen, 518060 China

[4], Department of Chemical Engineering, McMaster University, Hamilton, ON, Canada L8S 4L7

* Corresponding authors:
gangwu@buffalo.edu (G.W.); dsu@bnl.gov (D.S.); dhiggins@mcmaster.ca (D. H.)
[†]: These authors contributed equally

Abstract: The ever-increasing global environmental and energy crisis issues necessitates technological innovation, especially in the development of renewable energy-related devices, such as electrochemical energy conversion and storage technologies, including fuel cells, water electrolyzers, and CO_2 electrolyzers. Reliable and sustainable energy conversion devices are highly dependent on engineering of electrocatalysts. State-of-the-art electrocatalysts for these electrochemical conversion systems are usually platinum group metal (PGM)-based nanoparticles with high cost, which has sparked intensive research on atomically dispersed single metal site electrocatalysts for decreasing metal loadings and boosting catalytic efficiencies by taking advantage of their inherent electronic effects, quantum size effects, and metal-support interactions. In this review, we first introduced the intrinsic active site identification and stabilization, followed

by addressing the mutual metal-support interactions, and most important, their correlations with catalytic properties. Next, the advances in synthetic strategies and characterization techniques for single metal site electrocatalysts are highlighted. Recent advances in single metal site electrocatalysts designs for applications in electrochemical conversion reactions are also presented. Finally, remaining challenges and a forward-looking perspective on this field of research are provided.

Keywords: single metal sites, heteroatom doping, electrocatalysis; energy conversion; MOFs

Table of Contents

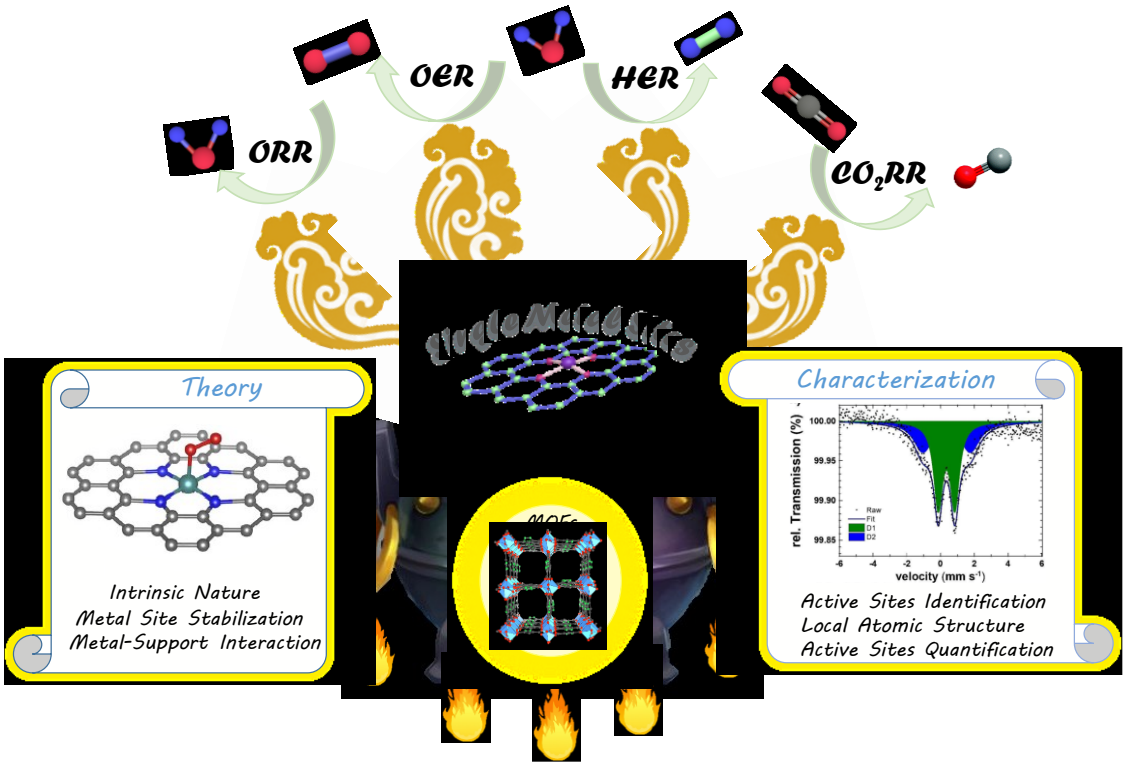

1. Introduction

Recently, the design of atomic scale nanomaterials has played a crucial role in developing sustainable energy-related technologies to address increasing environmental and energy challenges [1]. Particularly, nanomaterials with controlled surface, structural and electronic

properties are integral components of electrochemical energy conversion and storage devices, including fuel cells, rechargeable metal-air batteries, water electrolyzers and electrosynthesis technologies [2-8]. The performance of electrochemical conversion technologies relies on advances in nanoscience and nanotechnology, especially with regards to electrocatalyst engineering. Most state-of-the-art electrocatalysts are platinum group metal (PGM)-based nanomaterials [5, 8-13]. However, the high cost and scarcity of these PGMs has triggered extensive research on improving mass activities through composition and structural modification to reduce the amount of PGMs required to achieve target reaction rates, or the development of PGM-free metal catalyst alternatives [14-17]. Supported atomically dispersed and nitrogen coordinated single metal site electrocatalysts are an active and exciting area of research, owing to their unique characteristics that are advantageous from a catalysis standpoint [6, 18]. This includes: (i) The possibility of achieving 100% metal utilization due to the possibility of having all active metal atom sites on the surface of the catalyst (as opposed to some atoms being inaccessible in the bulk, as in the case of nanoparticles), which allows the reduction of metal content and consequently reduced catalyst cost; (ii) single atoms within a catalyst support can provide favourable adsorption and binding interactions with reactive species and catalytic intermediates to enhance overall reactivity; (iii) well-defined active site structures that emulate those of homogeneous catalysts that can achieve excellent selectivity [19], with the additional advantage that the active sites are immobilized on a solid support; and (iv) the ability to tune the electronic and adsorption properties of the active sites by modifying the metal center type, ligand structure, and nature of the support material. Single metal site electrocatalysts have emerged as promising materials for a variety of applications, particularly as efficient electrocatalysts for electrochemical reactions, including the oxygen reduction reaction (ORR), oxygen evolution reaction (OER), hydrogen evolution reaction

(HER), nitrogen reduction reaction (NRR), and carbon dioxide reduction reaction (CO_2RR) [2, 18, 20-26]. Therefore, highly active, stable and selective atomically dispersed and supported single metal site electrocatalysts will help perpetuate the development of many sustainable electrochemical energy technologies [20, 27-29]. The catalyst development requires the rational tuning of active site structures, configured to have optimized local coordination environments and surface adsorption properties. Probing the geometric and electronic configurations of active site structures in atomically dispersed supported single metal site electrocatalysts using advanced characterization techniques will play a significant role in understanding the underlying electrochemical reaction mechanisms, establishing structure-performance descriptors, and guiding the design of catalysts with high performance. Tracing the advances in single metal site electrocatalysts development in this decade, significant progress has been achieved toward following aspects:

(i) *Synthesis strategies for modulating the intrinsic activity and surface concentration of active sites.* A diversity of atomically dispersed single metal site electrocatalysts have been successfully synthesized, ranging from PGM atoms (*e.g.*, Au, Pt, Pd, Ru, Ir) to PGM-free atoms (*e.g.*, Fe, Co, Ni, Mn, Cu, Mo, W) anchored on a variety of support materials, including nanostructured carbons, boron/phosphorus nitrides, and metal oxides/carbides/nitrides/sulfides [30-35]. Furthermore, synthetic strategies have been implemented to significantly increase the surface concentration of active sites (*i.e.*, the number of catalytically active sites per unit surface area of catalyst material) [36-39].

(ii) *Structural and chemical insight into single metal site electrocatalysts through the development and implementation of advanced characterization techniques*. Advanced characterization techniques such as scanning transmission electron microscopy (STEM), X-ray

absorption near edge spectroscopy (XANES), X-ray absorption spectroscopy (XAS), and Mössbauer spectroscopy have provided an unprecedented level of understanding into the active site structures, including atomic configurations, local coordination environments, geometric configurations, ionic state and structural evolution [40-43].

(iii) *Insight into electrocatalytic reaction pathways and mechanisms on single metal site electrocatalysts using first principles density functional theory (DFT)*. Due to the homogeneity and straightforward configuration of active sites for atomically dispersed supported single metal sites, DFT calculations have been utilized for probing electrochemical reaction mechanisms [6, 19, 24, 42, 44, 45]. DFT calculations also serve as a valuable tool for screening active metal site structures and configurations for a variety of electrocatalysis reactions, such as predicting how reactant and the relevant intermediate adsorption energies (and thereby reactivity) vary with the metal-center type, coordination environments, and local carbon structures or defects in atomically dispersed supported single metal site electrocatalysts [28, 46-49].

In this review, we will focus on recent progress made in each of these important areas of research, along with providing a perspective on scientific opportunities for enhancing fundamental knowledge and realizing practical implementation of atomically dispersed supported single metal site electrocatalysts into electrochemical energy technologies, including fuel cells and electrolyzers. First, we will address the fundamental scientific principles underlying PGM and PGM-free-based atomically dispersed supported single metal site electrocatalysts, including the unique intrinsic characteristics and mutual metal-support interactions that influence reactivity. Second, synthesis strategies for enhancing the surface concentration of active sites will be summarized, followed by highlighting advancements in the use of characterization techniques to understand the structural and electronic properties of these materials. We will then discuss recent

progress in the development of single metal site electrocatalysts for a variety of important electrochemical conversion reactions. Finally, emerging scientific opportunities will be highlighted to provide guidance for the research community towards addressing global energy challenges through the development and implementation of new and high performance single metal site electrocatalysts.

2. Fundamental Basis

2.1 Characteristics of supported and coordinated single metal site electrocatalysts

By definition, supported and coordinated single metal site electrocatalysts are comprised of atomic metal atoms stabilized by heteroatom ligands (*e.g.*, N or O) and bonded with a support, possessing merits including the ability to achieve 100% metal utilization (i.e., all metal active sites can reside at the surface of the catalyst) and high selectivity, similar to their homogeneous catalyst counterparts [6, 42, 50]. The selectivity can arise largely due to the well-defined active structures and high degree of structural homogeneity in these catalyst materials. As the size of the metal clusters shrinks from bulk-scale to nanoparticles, and then to single atoms, the number of unsaturated low-coordination number atoms sharply increases. This leads to an increase in surface energy, which can provide remarkable catalytic activity enhancements, but comes with a high propensity for metal atom mobility and aggregation.

Design and engineering of single metal site electrocatalysts has been flourishing in the field of electrocatalysis recently, especially for ORR, OER, HER, NRR, and CO_2RR. However, despite significant progress, there are still several open questions that must be clarified through targeted scientific efforts: i) the impact of metal-support interactions with a focus on tuning these interactions to improve catalyst performance; ii) an in-depth understanding of the metal active sites formation for guiding the efficient synthesis of the atomically dispersed and supported single metal

site electrocatalysts; iii) an thorough illustration of the inherent atomic-level structure and properties of the active species that are responsible for the electrocatalysis; and iv) established structure-property-performance relationships that can correlate the results from rigorous (and ideally *in situ*) characterization of single metal site electrocatalysts with their intrinsic catalytic activity/selectivity, and their performance within an electrode structure (i.e., membrane electrode assembly-MEA).

2.2 Mutual metal-support interactions

Obtaining an understanding of the metal-support interactions in supported and coordinated single metal site electrocatalysts is of prime importance for elucidating the correlation between the characteristics of these catalysts and their catalytic performance. Metal-support interactions encompass the interplay between the atomic metal atoms and the host support materials. Namely, these interactions provide stabilizing effects and geometric/electronic effects, while dictating the overall active site concentrations that can be achieved. Furthermore, the introduction of atomically dispersed single metal atoms into catalyst supports can cause structural and electronic modifications to the support material such as carbon, which can in turn impact electrocatalytic performance. These topics will be discussed individually in the preceding sections.

Atomically dispersed metal atom coordination

In general, carbon materials, metal oxides/carbides/sulfides/nitrides, boron nitrides, or phosphorous nitrides can be used as effective supports for stabilizing noble metal atoms, as they commonly contain vacancies that can serve as trappers for single atom metal species [33, 35, 51, 52]. Positively charged noble metal single atoms could establish robust covalent bonding with the metal oxides/nitrides/carbides due to the more vacant *d*-orbitals, thus generating ultra-stable single metal site electrocatalysts with high reactivity [53-55]. It has been shown that metal oxides suffer

from poor electrical conductivity, which is disadvantageous for electrochemical reactions, and thus these materials are usually applied as catalysts in thermal heterogeneous reactions [52-54] or needed to add conducting additives. Oppositely, carbon materials and many metal carbides/nitrides can provide intrinsic conductivity, and have therefore been used as supports for noble metal single atoms for electrocatalysis reactions [32, 33].

Heteroatom (N, S, or P etc.) doped carbon materials like graphene, carbon nanotubes or other carbon precursor (*e.g.*, pyrrole, dicyandiamide, glucose, dopamine etc.) derived supports are the most commonly used matrices for anchoring single metal atoms through coordination with defects, N-containing groups or unsaturated coordination sites. Graphene, with a simple structure that can contain multiple-defect structures including single vacancies (SV), double vacancies (DV), pyridinic and pyrrolic coordination site, is regularly used for anchoring atomically dispersed transition metal atoms [46]. As displayed in **Figure 1**A, different kinds of defects in carbon supports could provide the anchoring sites for single metal atoms. They possess different atomic configurations and 3d orbital electron density, impacting the intrinsic catalytic activities. A diversity of active site motifs could be obtained through metal atom bonding with different defect types, thus favoring a variety of reaction kinetics. For example, atomically dispersed Ni atoms embedded in SV (Ni@SV) and DV (Ni@DV) are more active for electrocatalysis toward CO_2RR than HER in neutral medium, while the Ni atoms coordinated in D5775 carbon defects (Ni@D5775) is highly selective for OER catalysis in alkaline electrolyte and HER in acidic electrolyte [56].

In Fe-N-C catalysts, porphyrin-like FeN_4C_{12} structures are generally identified as the active sites, present in micropores either in the disordered nanosheets or between the zigzag edges of graphitic carbon structures [18, 49, 57]. DFT calculations manifested two possible adsorption

modes of dioxygen on FeN_4C_{12} moieties through the end-on or side-on configuration [57]. DFT calculation results confirmed that the end-on type was preferred, resulting in a displacement of Fe(II) out of the graphite plane. Further insight into the catalyst performance was obtained by virtue of *in situ* XANES spectroscopy. It was observed that not only the ORR electrocatalysis arose from electrochemical potential dictated between high-spin O_x-Fe^{3+}-N_4 to nonplanar HO-*Fe^{2+}-N_4 (Fe atoms shifting away and toward the N_4 plane) [58-60]. Following this work and employing the same synthesis strategies, three defective CoN_x moieties were identified, including CoN_4C_{12}, $CoN_3C_{10,porphyrinic}$ and CoN_2C_5 for ORR, OER and HER catalysis in acidic electrolyte [61]. The weaker adsorption energy toward O-containing intermediates on CoN_x than FeN_x species explained their inferior ORR catalytic activity. It is commonly believed that Co-N-C catalysts shared identical catalysis mechanism to Fe-N-C catalysts toward ORR catalysis. However, the redox potential of Co moieties are above 1.0 V versus RHE, outside the range of ORR square-wave voltammetry test window, rendering the exact catalytic path still ambiguous [62]. But, as a bifunctional active site, the OER process of Co site was associated with an Co ion oxidation shift. For instance, dioxygen formation were enabled by a side-on hydroperoxo ligand on as-generated Co^{4+} active sites through a sequential charge conversion $Co^{2+} \rightarrow Co^{3+} \rightarrow Co^{4+}$ [63].

Metal organic frameworks (MOFs), consisting of metal nodes connected with nitrogen-enriched organic ligand linkers, such as Zn-based zeolitic imidazolate framework (ZIF)-8 and Co-based ZIF-67, are other commonly used metal/nitrogen/carbon precursors for synthesis of single metal site electrocatalysts [4, 20, 23, 64-69]. Benefiting from their intrinsic high porosity, well-defined MOF derived carbon materials usually possess a high surface area, enabling the immobilization of a variety of metal single atoms. For example, Ru single atoms were successfully anchored into MOF structures through a strategically cage-controlled encapsulation followed by *in-situ* reduction

of Ru precursors in the porous channels of the MOF [70].The unique confinement effect provided by the porosity of MOFs yields a stabilization effect and aids in achieving a homogeneous distribution of active sites. In addition to the widely studied Fe-N-C [23, 71], Co-N-C [64, 72, 73], and Mn-N-C [20] catalysts, new catalyst configurations have also emerged, such as Cu-N-C [74] and W-N-C [75]. Besides, MN_1, MN_2 or MN_3 moieties have also been proposed as active sites for electrochemical reactions [21, 25, 75-77]. FeN_2 [21] and Mn-N_3O_1 [77] moieties-rich carbon catalysts for the ORR were also reported. The enhanced catalytic activity mainly originated from the down shift of *d*-band center relative to Fermi level that optimized the adsorption and desorption energy toward reaction intermediates according to Sabatier's principle.

Atomic Configuration — Geometric and Electronic Effects

It is postulated that the local environment of the metal atom active centers dominates the intrinsic activity, selectivity and stability of single metal atom catalysts through regulating the electronic and geometric configuration. The electronic effects (e.g., electron distribution, charge density accumulation and mobility) and geometric effects (e.g., tensile or compressive strain, or out of plane/in plane configurations) induced by inserting metal single atoms into support materials plays a primary role in altering electronic conductivity or *d*-band center shifts [42, 50, 78]. This plays a significant role in affecting catalytic performance, as these modifications tune adsorption energies that are neither too strong nor too weak towards key reaction intermediates. A number of studies [79-81] have reported that the electron withdrawing character of the carbon support plays a vital role in affecting the electron density of metal center. As depictured in **Figure 1B**, the intrinsic activity of active sites will be altered based on their electron withdrawing properties. It is believed that this property could contribute to a higher activity of Fe-N-C catalysts by inducing an anodic shift in the redox potential between Fe^{2+} and Fe^{3+}.

Inserting additional guest atoms such as sulfur or phosphorous atoms into atomically dispersed metal atom catalysts could further modify the electronic and geometric configurations of the active sites. For example, as reported by Chen and co-workers, the electronic structure of Fe single atoms embedded in N, S and P co-doped hollow carbon polyhedron was adjusted by the near-range coordination with N atoms and long-range interaction with S and P atoms, resulting in a less positive charge of Fe ($Fe^{\delta+}$) and thus a weaker affinity to ORR intermediates (OH*) [22]. Similar conclusions were also made by Li et al., who hypothesized that the introduction of S atoms induced a negative charge on neighboring N atoms, thereby weakening the binding energy with adsorbed OH* species for enhanced ORR catalysis in alkaline medium, as depicted in **Figure 1C** [82]. The effect of S-doping for inducing uneven distribution of charges for bifunctional ORR and OER electrocatalysis was investigated, which an additional role of S-doping in enlarging the surface area of carbon materials was shown possible via pore generation through the readily removed FeS species [83-85]. In a different case, the promoted reaction kinetics for OER and CO_2RR are derived from the elevated electron transfer rate triggered by the formation of Ni-N-S or Fe-N-S active sites in carbon matrix [29, 86]. Aside from charge redistribution for regulating reactant intermediate adsorption energies, inserting metal atoms could also induce local geometric deformations. As postulated by Ling and co-workers, implanting Ni single atoms onto β_{12}-boron monolayer bended the surrounded surface of the flat β_{12}-boron monolayer and induced tensile strain, leading to the decreased adsorption energy toward H* adsorption for HER electrocatalysis, as described in **Figure 1D** [87].

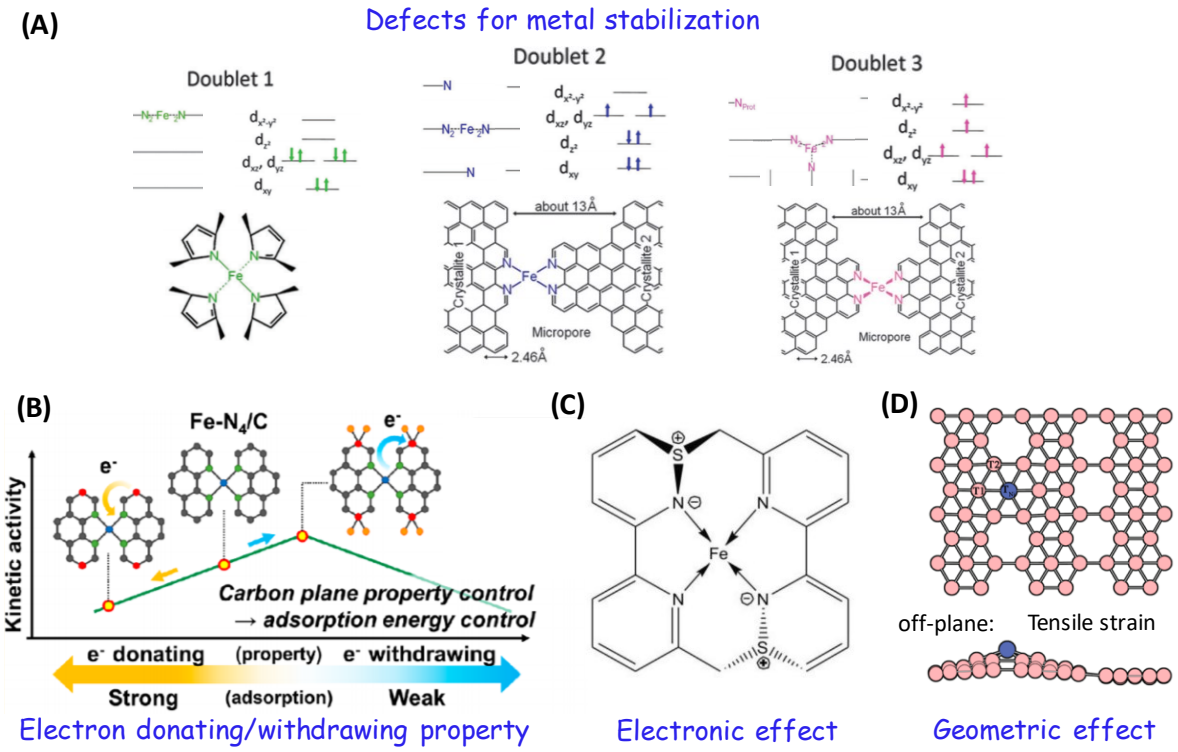

Figure 1. (A) Schematic demonstration of the defect stabilization effect for anchoring FeN_4 active sites in graphene and their top-view, side view and electron density. Reproduced with permission from ref [88]. Copyright 2012, American Chemical Society. (B) Schematic illustration of the electron withdrawing property for adjusting the adsorption energy towards the reaction intermediates. Reproduced with permission from ref [89]. Copyright 2019, American Chemical Society. (C) Electronic effect induced by introduction of S atoms to the carbon support. Reproduced with permission from ref [82]. Copyright 2018, WILEY-VCH. (D) Geometric effect caused by inserting Ni single atoms in boron monolayer. Reproduced with permission from ref [87]. Copyright 2017, American Chemical Society.

Correlating Electrocatalytic Performance with the Properties of the Active Sites

Universal design principles for guiding electrocatalyst engineering efforts are generally established by identifying correlations between the properties of the catalytically active sites and their intrinsic activities, and advanced efforts are still needed in this area. Hu and co-workers conducted a thorough study using graphene-supported atomically dispersed electrocatalysts for different reactions [46]. They reasonably postulated a universal descriptor, φ, for connecting the intrinsic properties of active centers (electronegativity and coordination environment) with their catalytic activities, given the following equation:

$$\varphi = \theta_d \times \frac{E_M + \alpha \times (n_N \times E_N + n_C \times E_C)}{E_{O/H}} \ ,$$

Where, E_M, E_N and E_C represent the electronegativity of metal, N and C elements, respectively. N_N and N_C represent the number of nearest neighbor N and C atoms, respectively. α is the correction coefficient with value of 1.25 for transition metal single atoms-pyrrole-N_4 and 1.0 for other active sites. This descriptor was shown capable of predicting the catalytic activities of transition metal single atoms coordinated with pyrrole-N_4 and supported on graphene through calculation of related reaction adsorbates (OH* and H*). The results are highly consistent with the experimental data that Fe-, Co- and Mn-pyrrol-N_4 for ORR, OER and HER, respectively, as plotted in **Figure 2**, underscoring its substantial significance in optimizing the synthesis of active sites of single metal site electrocatalysts on graphene.

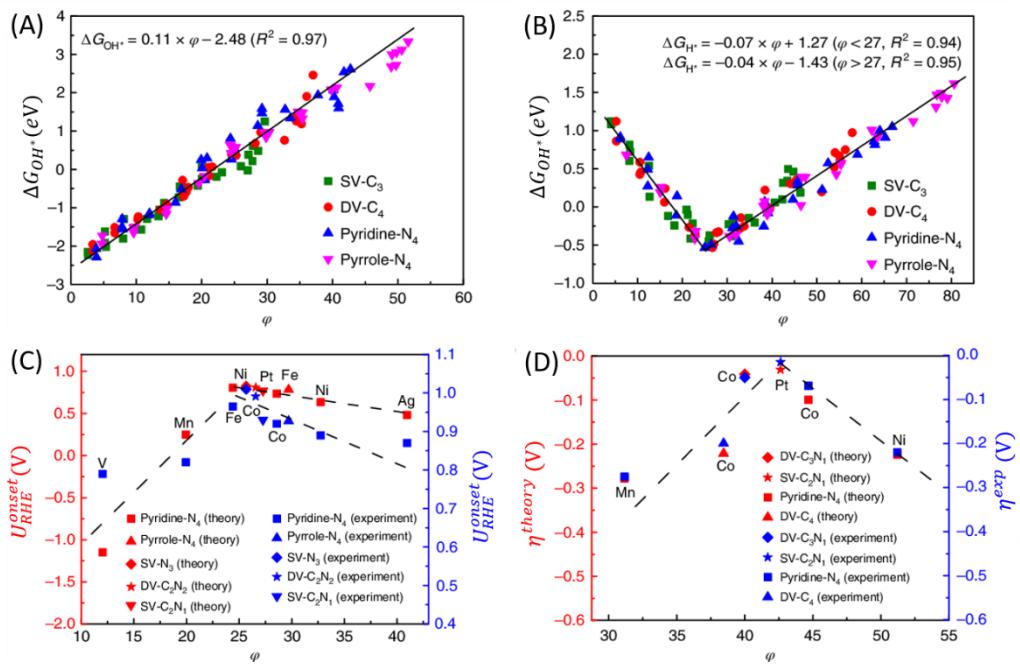

Figure 2. Plots of the relationships of (A) ΔG_{OH*}, (B) ΔG_{H*}, (C) onset potentials for ORR electrocatalysis, (D) overpotentials for HER of transition metal single atoms supported on graphene with the descriptor φ. Reproduced with permission from ref [46]. Copyright 2018, Springer Nature.

Surface Concentration of Active Site

Quantifying the surface concentration of active sites is of primary importance, yet quite challenging for evaluating the intrinsic activity of the electrocatalysts, reflected by the value of turnover frequency (TOF, TOF=j_k/(S_{BET}*D_{atom}*W_{site}*m) [90], where, j_k is the kinetic current density; S_{BET} is the BET surface area; D_{atom} is the carbon atomic density; W_{site} is the atomic ratio of active sites; m is the mass loading on electrode). For detecting single metal sites in M-N-C catalysts, especially in Fe-N-C electrocatalysts, KSCN and H_2S are commonly used as poisons for electroanalytical strategies due to their strong adsorption. Advanced characterization techniques

such as ^{57}Fe Mössbauer spectroscopy [91] combined with low-temperature CO chemisorption has also been shown effective for quantifying active sites [92], and is a strategy discussed in detail in the next section of this review dedicated to catalyst characterization.

3. Innovative synthesis approaches

Well-defined atomically dispersed supported single metal site electrocatalysts hold great promise in energy-related applications, which relies on development of reliable and rational synthesis strategies. Methods such as mass-selected soft landing [93], O_2 plasma[94], or atomic layer deposition [95, 96] could enable the precise atomic-level control to achieve dispersed metal atoms for theoretical studies, yet the practicality for mass production must be carefully considered as these techniques commonly have low synthetic yields and require sophisticated equipment. The most popular wet-chemistry approaches are usually multi-step, involving precipitation, impregnation, deposition or adsorption of metal precursors onto support materials, followed by pyrolysis or heat treatment for attaining homogeneously dispersed metal atoms embedded within the catalyst support. To avoid redundancy with previously published review papers dedicated to this topic [6, 42, 44, 50, 78], we first present an example of how understanding the atomic and geometric structure evolution to guide the rational synthesis of single metal site catalysts with high intrinsic activity has been used, then will focus more on the methods for enhancing the surface concentration of active sites and on efforts to scale-up production, which are key barriers to achieve the practical implementation of single metal site electrocatalysts in electrochemical energy technologies.

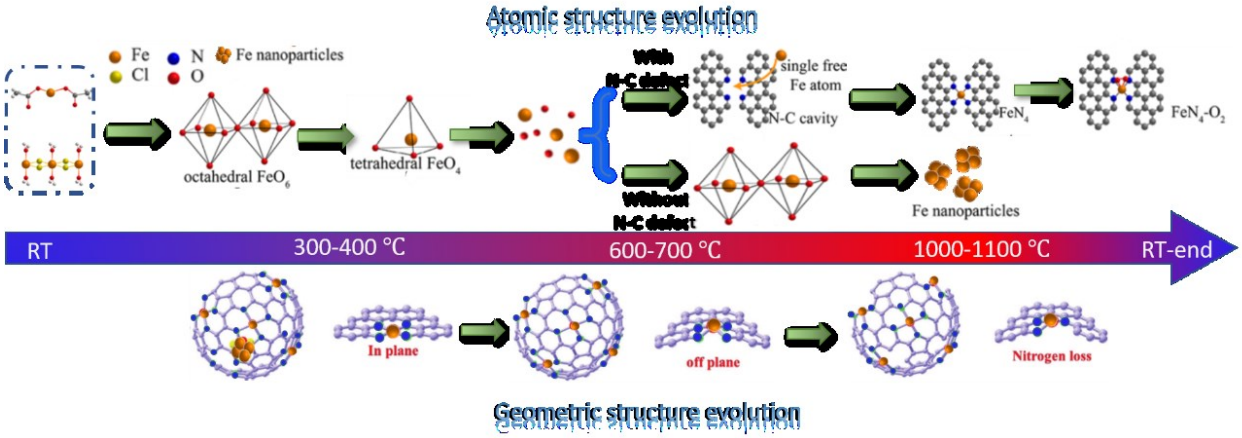

Figure 3. Thermal-driven formation of Fe-N_x moieties: (upper) atomic structure evolution; Reproduced with permission from ref [97]. Copyright 2019, American Chemical Society. (down) geometric structure evolution. Reproduced with permission from ref [98]. Copyright 2019, WILEY-VCH.

The most studied class of materials is Fe-N-C catalysts, including investigations into metal center formation mechanisms, atomic configurations, reaction intermediate adsorption modes and activity degradation mechanisms. All of these studies are of vital importance in directing the rational synthesis of highly efficient Fe-N-C electrocatalysts as well as offering hints for other M-N-C catalysts synthesis. A common consensus toward the formation FeN_4 moieties was reached using in situ temperature ramp XAS monitoring.[97] During the pyrolysis process as shown in **Figure 3** (top), the atomic structure of Fe-N-C catalysts goes through a thermal-driven pathway: i) Fe precursors; ii) octahedral Fe-O_6; iii) tetrahedral Fe_1(II)-O_4; iv) single Fe atoms; and v) Fe_1(II)-N_4. During the structure evolution, N-C defects are crucial for capturing single Fe ions. Without them, the Fe-based nanoparticles would form. One finding of this study was that Fe precursors could either be Fe salts or Fe-oxides, which could decompose into free Fe ions during the pyrolysis process. This may open an avenue for vapor phase synthesis of atomically dispersed single metal

site electrocatalysts. Li et al. proposed a much lower pyrolysis temperature of 400 ℃ is sufficient for generation of FeN_4 sites when using ZIF-8-derived carbon as a host to adsorb Fe^{3+} ions from $FeCl_3$ [98]. Modeling simulations further suggested that N-C defects in carbon are able to stabilize free isolated Fe ions and form FeN_4 structure in order to reduce the system energy. In addition to the atomic structure evolution, the geometric structure of the bonding length/strength between Fe-N bonds evolved with increasing pyrolysis temperatures. As depicted in **Figure 3** (bottom), the as-embedded FeN_4 moieties initiated a small local contraction strain by shifting from in-plane to out-of-plane within the carbon layer, which is kinetically favorable for decreasing the activation energy of breaking the O-O bond [98]. The geometric structure evolution offers guidance for adjusting the intrinsic activity of the active sites through tuning their covalent bonding length through tuning thermal activation conditions.

Obviously, achieving a higher surface concentration of active sites would boost the performance of single metal site electrocatalysts. Tactfully devised synthesis strategies have been shown to have remarkable success in increasing the loading of metal single atoms up to 20 wt% [99, 100] without observing significant metal nanoparticle formation or agglomeration. The key to these strategies is either increasing the number of chelating sites (*e.g.*, N dopants) available to host metal single atoms, or strengthening the atom trapping or stabilizing ability of the chelating sites on the catalyst support surface. Increasing the surface concentration of active sites using conventional wet-chemistry methods is difficult due to the propensity for metal atom migration or aggregation during the synthetic process, especially during high temperature (>700 ^{o}C) pyrolysis procedures. An additional challenge is that many synthetic procedures could not generate enough anchoring sites (e.g., nitrogen doping and metal content, defects, uncapped sites etc.) for capturing the metal precursors and hosting them in the support. Research efforts dedicated to overcoming

this challenge have involved the development of novel synthesis strategies that include steric confinement methods, anchoring sites creation, acid leaching and thermal gas-migration strategies, which are outlined below.

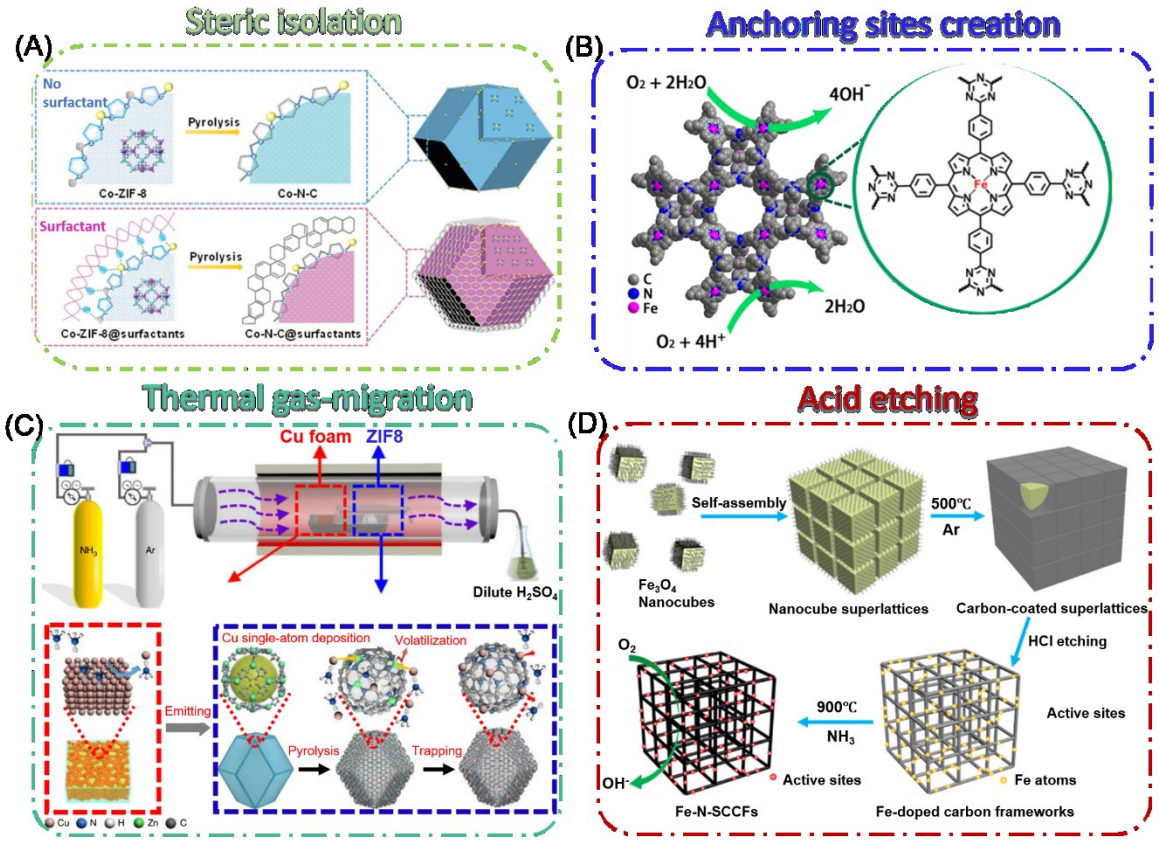

Figure 4. (A) The confining effect of surfactant for synthesis of Co-N-C electrocatalysts using F127 as isolation agent. Reproduced with permission from ref [64]. Copyright 2019, The Royal Society of Chemistry. (B) Molecular structure and characterization of Fe Single atoms/PTF-600. Reproduced with permission from ref [101]. Copyright 2018, American Chemical Society. (C) Thermal gas-migration strategy for scale-up synthesis of Cu-N-C catalysts. Reproduced with permission from ref [74]. Copyright 2018, Springer Nature. (D) Top-down acid etching strategy for fabrication of Fe-N-C catalysts. Reproduced with permission from ref [102]. Copyright 2017, American Chemical Society.

Steric confinement strategies, also called “isolation” or “fencing” strategies, employ a ligand or a secondary atom that physically prevents metal atoms in the precursor mixtures from contacting each other, thereby prohibiting migration and aggregation. This steric confinement is a key advantage of using metal-substituted zinc-rich ZIF-8 as a precursor, which chelates the metal atoms with nitrogen containing ligands, and maintains separation between them with Zn species [20, 27, 62, 64, 73, 103]. The Zn atoms are then removed by evaporation during a pyrolysis (*i.e.*, > 900 ℃) procedure. Other atoms such as Na, K, Li, Mg, and Al are also capable of playing a similar role as the Zn atoms, with the benefit that they can be easily washed away after pyrolysis [104, 105]. In addition, these zinc compounds that are removed either during or after pyrolysis can act as pore-forming agents, resulting in enlarged surface areas through the creation of nanopores during their removal. Some block polymers, like Pluronic F127 and polyvinylpyrrolidone, could also serve as complexing agents to maintain steric separation between active metal atoms. He et al., reported a doubling of CoN_{2+2} active sites concentration as a result of the confinement effects of F127 on the surface of Co-doped ZIF-8, in comparison to that of catalysts prepared in the absence of the F127 as shown in **Figure 4**A [64]. The protection of the block polymer is able to suppress both Co atom agglomeration and internal micropore collapse. 1,10-phenanthroline (Phen) ligands have also been used as an isolation agent for promoting the complete transformation of Fe precursors into single Fe atom active centers, which resulted in a high concentration of active sites up to 3.5 wt% [36]. Another representative work was reported by Zhao *et al*. [37], who devised a cascade anchoring tactic for obtaining a high concentration of metal loading up to 12.1 wt%. This synthetic method involved multiple isolation steps, in which excessive amounts of glucose were employed as the isolation agent for securing the atomic dispersion of metal atoms. At first, glucose

acted as both a chelating agent to sequester metal ions by bonding with O-rich functional groups on the carbon support, and as a protection agent for protecting the as-formed metal complexes from agglomerating through physical isolation. Then, during the subsequent pyrolysis for formation of MN_x moieties, the residual glucose stabilized the metal complexes from migration and aggregation. The versatility of this synthesis strategy was demonstrated by its use for preparing single metal site electrocatalysts with M-N-C configurations (M=Fe, Co, Ni, Mn, Cu, Mo etc.) via tuning chelation agent, carbon substrates and metal sources for a broad range of applications [37].

Traditional pyrolysis of N-containing carbon precursors in the presence of transition metal species to facilitate covalent metal-nitrogen (MN_x) bonding is usually limited by the insufficient availability of nitrogen site (less than 5 at.%) for chelating the metal ions into catalytically active sites. An approach to overcome this challenge relies on the selection of precursors that can form sufficient concentration of nitrogen doping sites for anchoring single metal sites. For example, covalent triazine frameworks composed with four pyrrolic N sites in trimerization of aromatic nitriles are capable of offering anchoring sites for grasping metal ions, as illustrated in **Figure 4B** [101]. Covalent triazine frameworks for anchoring metal single atoms through an ionothermal approach was demonstrated capable of increasing the concentration of FeN_4 active sites to 8.5 wt% [101]. In another work, Cheng and co-workers [99] took advantage of the abundant six folds cavities of g-C_3N_4 that formed *in situ* when dicyandiamide was used as a precursor for carbon nanotube growth. Under the first-step pyrolysis process, Ni-O-C on the melem (2,5,8-Triamino-tri-s-triazine) skeleton were formed through condensation reaction of dicyandiamide at 350 ^oC, and then the Ni single atoms were effectively confined in g-C_3N_4 six fold cavities at 650 ^oC during the second-step pyrolysis. The loading of dispersed Ni single atoms was increased up to 20 wt% after the third-step pyrolysis at 700-900 ^oC. Nevertheless, it is surprising that such a high loading

of Ni single atoms can be obtained without the observation of Ni nanoparticles, particularly because Ni nanoparticles are generally the catalyst for carbon nanotube growth [106]. This could be due to the subsequent decomposition of nanoparticle into atomically dispersed single sites given sufficient ligands are provided. Even higher metal concentrations using the same carbon source were achieved [100] by a facile liquid phase deposition method employing dicyandiamide for chelating single Cu atoms, whereby metal concentration as high as 20.9 wt% were obtained. However, it should be noted that the effective metal sites should be at the surface available for electrochemical reactions, rather than embedded under supports.

Another effective strategy of enhancing metal concentration and scale-up production is the thermal gas-migration method [107], where Pt atoms were emitted from bulk Pt during a high-temperature heat treatment, and were subsequently trapped by the oxygen vacancies in supports such as CeO_2. Inspired by this success, ZIF-8 precursors were used as a trapper for capturing emitted Cu atoms from a copper foam for a scaled-up production of single Cu site catalysts [74]. As illustrated in **Figure 4C**, ammonia molecules would complex with Cu atoms to form $Cu(NH_3)_x$ complexes through Lewis acid-base interactions [74]. Then, the N-containing species in the carbon support matrix can trap $Cu(NH_3)_x$ complexes, causing the homogeneous formation of isolated ionic Cu sites with valence state between Cu(II) and Cu(0) on Cu-N-C catalysts. The evaporation treatment time was found crucial for minimizing the generation of Cu nanoparticles. The calculated surface coverage of single Cu atoms was approximately 0.06 atom/nm^2 based on inductively coupled plasma (ICP) emission spectroscopy and Brunauer-Emmett-Teller (BET) surface area analysis. Another successful demonstration is the synthesis of atomically dispersed Pt single atoms on defective graphene, which was studied as the HER and selective oxidation of different organosilanes [36]. This straightforward thermal gas-migration strategy avoids the multi-

step synthesis procedure often used in traditional wet-chemistry methods involving metal ion adsorption/impregnation, washing, and pyrolysis procedures. Therefore, this direct and facile synthesis method has shown a great promise for the production of single metal site electrocatalysts with a high content of homogeneously dispersed metal single atom active sites.

In addition to thermal emitting procedures, acid leaching of metal and carbon containing materials is another top-down strategy for achieving highly porous catalysts with a high concentration of active site by using metal or metal oxide species as hard templates. A new type of highly ordered and graphitized Fe-N-C catalysts was previously prepared by *in situ* carbonization of ligands covering the surface of self-assembled Fe_3O_4 nanocube superlattice templates [102]. Following this carbonization, which formed a thin film of carbon coating on the Fe_3O_4 nanocubes, the Fe-oxide nanocubes were removed by leaching with HCl, and the resulting materials were heat treated at 900 °C in NH_3 (**Figure 4D**). In this way, the Fe_3O_4 not only served as a source of Fe ions for the formation of atomically dispersed active site structures, but also served as a hard template for the formation of well-ordered, high surface area catalyst structures [102]. The concentration of Fe active sites is about 1-2 wt%, and the high homogeneity and long-range ordered nanoporosity provided favorable mass transport properties during the ORR. It should be noted that a high concentration of active sites doesn't guarantee good catalytic performance. First, the intrinsic activity (i.e., turnover frequency of the active sites) must be maximized through modifications to the electron configuration, local coordination environment, and metal support interactions as discussed in section 2. Furthermore, improving reactant accessibility to the atomically dispersed active site structures is another essential requiring for high performance electrocatalysts [102, 108, 109].

4. High-resolution characterization for atomically dispersed and supported metal sites

Structural characterization is important for gaining insight into the atomic configurations, the support properties, and the metal-support interactions occurring in single metal site electrocatalysts. This understanding is essential for elucidating structure-property-performance relationships of this class of catalyst, which can be used to guide designs of advanced performance materials. X-ray-based spectroscopy approaches, such as X-ray absorption spectroscopy (XAS) and X-ray photoelectron spectroscopy (XPS) have been used to study the electronic properties of the atomically dispersed metal atoms in catalysts [20, 30, 64, 110-112]. Advanced aberration corrected high resolution STEM provides the capability to structurally image single metal site at the atomic scale, as well as obtaining chemical information through STEM enabled techniques, including STEM electron energy-loss spectroscopy (STEM-EELS) and STEM energy dispersive X-ray spectroscopy (STEM-EDX). Combining high resolution STEM imaging and quantitative spectroscopy has enabled advanced understanding on single metal site electrocatalysts [20, 23, 27, 30, 54, 111, 112]. Other techniques, such as ^{57}Fe Mössbauer spectroscopy (for Fe single metal site electrocatalysts) [57, 58] and scanning tunneling microscopy (STM) also used for exploring local environment of single metal sites [113]. In this section we will introduce the applications of XAS, XPS and STEM techniques on the characterization of single metal site electrocatalysts.

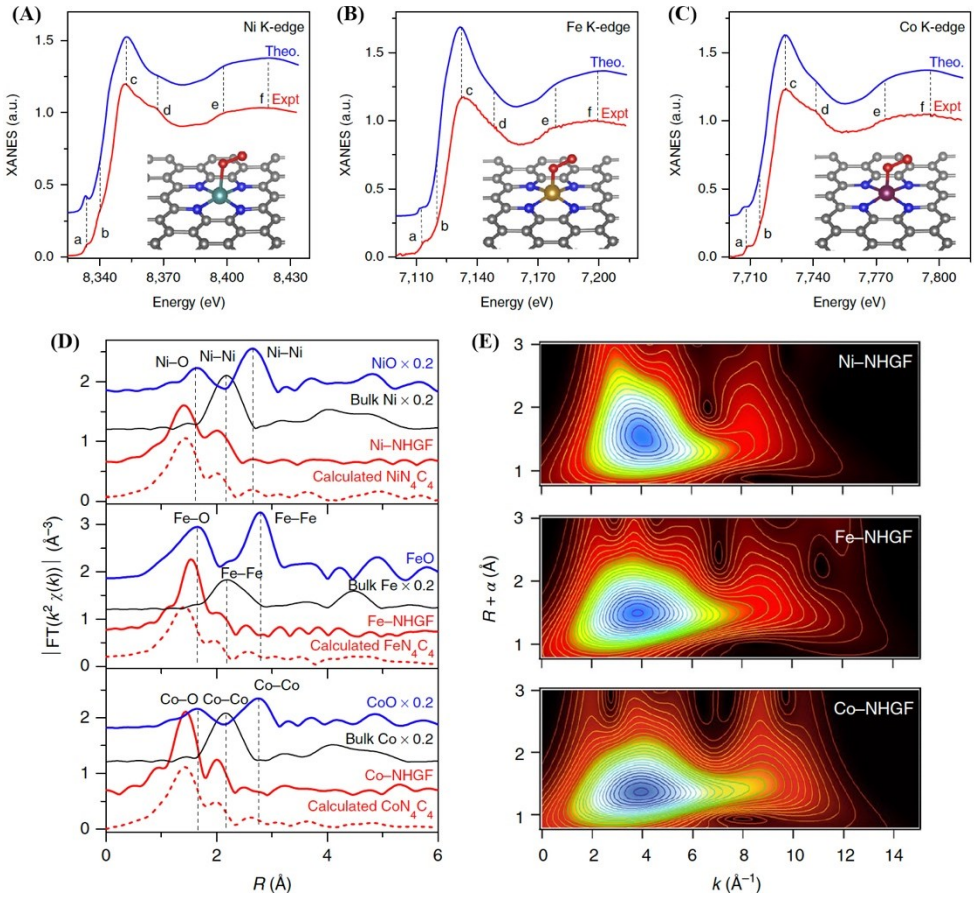

Figure 5. Comparison between the experimental (A) Ni, (B) Fe and (C) Co K-edge XANES spectra of M- nitrogen-doped holey graphene frameworks (NHGFs) and the theoretical spectra calculated based on MN_4C_4 moieties embedded in a 2D graphene lattice; (D) Fourier transformed EXAFS spectra of the experimental K-edge signals of M-NHGFs along with reference samples (solid lines). The dashed lines represent calculated spectra based on a divacancy-based MN_4C_4 moiety enclosed in the graphene lattice. The Fourier transforms are not corrected for phase shift; (E) Wavelet transforms for the k3-weighted EXAFS signals of M-NHGFs with optimum resolutions at 2.0 Å. The maxima at approximately 4.0 $Å^{-1}$ are associated with the M-N/O/C contributions. Reprinted with permission from ref [30], Copyright 2018, Springer Nature.

4.1. XAS to determine local coordination of single metal sites

XAS is based on an excitation of electrons in an atom from their initial core level to the lowest unoccupied state, thereby probing the density of unoccupied states [41]. XAS spectra can be divided into two parts according to the energy range: X-ray absorption near edge structure (XANES) and extended X-ray absorption fine structure (EXAFS). The XANES region (±50 eV relative to the absorption edge) gives chemical information such as oxidation states and coordination symmetry of the absorbing/excited atom. The EXAFS region (40 to 1500 eV beyond the absorption edge) gives structural information, such as coordination number, environment and bond distances [43]. Therefore, both regions can be analyzed to understand the chemical states and atomic structures of single metal atoms in catalysts, and XANES and EXAFS have become standard techniques for characterization of these materials [20, 30, 110-112].

XANES and EXAFS have been applied to track the structural evolution from Pt single atoms into nanoparticles during heating [114]. At 523 K, it was found a strong peak near 1.9 Å in EXAFS, which indicates only heteroatoms (here, sulfur) are around Pt atoms. In other words, Pt atoms are atomically distributed without a Pt-Pt bonding. As temperature increases (to 873 K), an evolution of a peak near 2.8 Å emerged, which originated from the 1st nearest Pt-Pt metallic bonding as a result of Pt agglomeration. By comparing the 1st nearest bonding distance around Pt, it was possible to demonstrate the structural change from single atoms to bulk particles, demonstrating the effectiveness of using EXAFS to probe single-atom dispersion. **Figure 5**A-E shows the XANES and EXAFS analysis on a series of atomic 3*d* metals (M: Fe, Co, Ni) in nitrogen-doped holey graphene frameworks (NHGFs), which were prepared by hydrothermal treatment with an aqueous suspension of graphene oxide, metal precursors, and H_2O_2, followed by freeze drying and annealing at 900 °C with flows of Ar and NH_3. These M-NHGFs were demonstrated as catalysts

for the OER.[30] Experimental XANES and EXAFS results, coupled with spin-polarized DFT simulations, corroborated that, in all of the materials, the transition metals had the same coordination environment, being present in the form of MN_4C_4 moieties. In addition, XAS can be used to probe the local arrangement around several elements in one catalyst. Zeng *et al.* examined EXAFS of Pt and Fe then suggested a single-atom to single-atom grafting of Pt onto Fe-N_4 center [103]. The unique active moiety of Pt_1-O_2-Fe_1-N_4 may provide much improved ORR stabilities as well as OER and HER catalytic activities.

4.2. XPS to determine heteroatom doping and interaction with metal sites

XPS is a near surface sensitive technique, which provides both quantitative and qualitative information on the chemical bonding of atoms within the near-surface region [40]. Chemical shifts of electron binding energies of a certain element reflect a change in the oxidation state and/or local chemical environment. The composition of each element can be deduced based on a linear relationship between the intensity of the signal from a certain element and its atomic concentration [115]. Thus, XPS has been widely employed for probing bonding states and near-surface concentrations of single metal atom active sites, as well as the atoms surrounding these structures.

As for the heteroatom such as nitrogen coordinated single metal site catalysts, XPS is necessary for determine the nitrogen doping in terms of their position and concentration. The nitrogen-doped carbon materials obtained from high-temperature pyrolysis often contains two major nitrogen species: pyridinic N (~398.6 eV) at the edge of carbon planes and graphitic N (~401.1 eV) at the interior of carbon planes, which can be easily discriminated by using XPS according to their significantly different binding energies [116-118]. Pyridinic N was considered as the critical ligand to stabilize single metal sites to form MN_x moieties, while graphitic N is able to modify the electron structure of carbon and adjacent metal sites. Although it is still under a debate, XPS analysis also

can be used to determine the relatively content of MN_x sites in catalysts. In an atomically dispersed CoN_4 catalysts derived from surfactant-assisted ZIF-8 precursors [64] showed that N 1s XPS signal was composed of four different N bonding configurations: pyridinic-N, graphitic-N, oxidized graphitic N, and Co-N_4. The contribution of Co-N_4 was found variable with different surfactants used during the synthesis, indicating the pluronic F127 block copolymer was the most favorable surfactant to form Co-N_4 sites with the highest density. In addition, XPS analysis was often used to quantitatively determine element content in the surface layers of catalysts and provides appropriate estimation of metal doping content and possible impurity.

4.3. Aberration corrected STEM to identify single metal sites

In addition to X-ray based techniques, high resolution high-angle annular dark-field scanning transmission electron microscopy (HAADF-STEM) with aberration correction can provide atomic level real-space information on single metal sites in catalysts. Compared to high-resolution TEM imaging, HAADF-STEM enables identification of heavier atoms (i.e., transition metals) within a sample comprised of mainly light elements (i.e., carbon supports), as the contrast of atoms in HAADF-STEM images is highly dependent on the atomic number (proportional to $Z^{1.7}$, where Z is the atomic number). For example, HAADF-STEM has been used to resolve 3*d* transition metal atoms supported on carbonaceous materials, or noble metal atoms supported on 3*d* transition metal oxides [23, 27, 111, 119, 120]. However, distinguishing 3*d* or 4*d* transition metal atoms supported on metal-oxides with a high Z-number (*i.e.,* Fe on CeO_2 or Pd on CeO_2) can be very challenging. Alternatively, one can perform atomic resolution spectrum imaging using either STEM-EELS or STEM-EDX to identify the presence of atomically dispersed single atoms on the metal oxide support materials [120]. As STEM-EELS and STEM-EDX measurements usually require a longer time to collect the signal (tens of seconds to tens of minutes) as compared to HAADF imaging,

electron beam effects should be considered when using these techniques. Ideally, one can reduce the beam effects by lowering the voltage of electron beam and reducing the beam intensity.

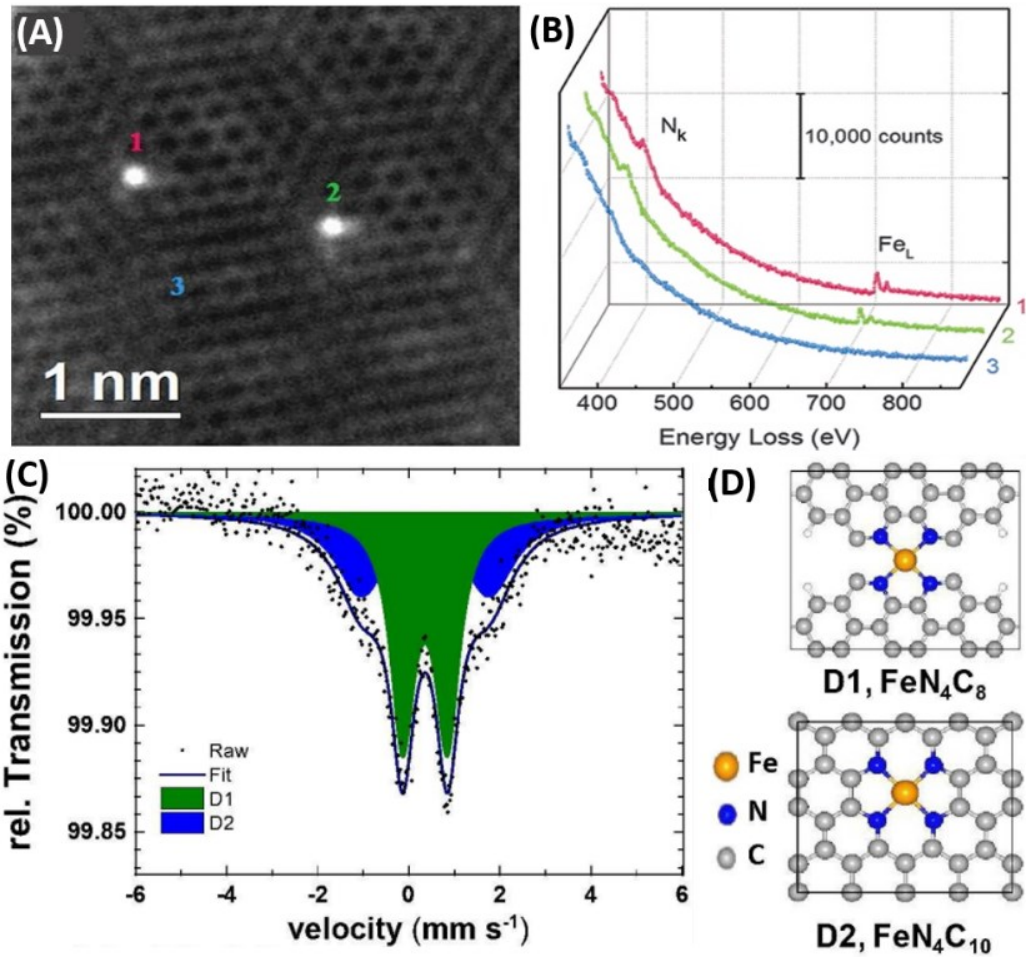

Figure 6. (A) HAADF-STEM image of individual Fe atoms (labeled 1, 2, and 3) in a few-layer graphene sheet; (B) EELS spectra of the N K-edge (N_k) and Fe L-edge (Fe_L) acquired from single atoms (1 and 2) and few-layer graphene (3), demonstrating the presence of N around the Fe atoms. Reproduced with permission from ref [119]. Copyright 2017, American Association for the Advancement of Science. (C) ^{57}Fe Mössbauer spectroscopy fitting of the Fe-N-C catalysts derived from Fe-ZIF8; (D) The local atomic configuration of Fe active sites: FeN_4C_8 (D1) and FeN_4C_{10} (D2). Reproduced with permission from ref.[91] Copyright 2019, The Royal Society of Chemistry.

Atomic-scale STEM imaging and the related spectroscopic techniques (EELS and EDX) have proven invaluable for evaluating whether catalyst materials consist of atomically dispersed single metal atoms, metal/metal-oxide nanoparticles, or both. One example of STEM analysis is shown in **Figure 6**A and B, displaying single Fe atoms anchored on a high surface area nitrogen-doped carbon support (Fe-N-C) [119]. STEM-HAADF imaging enabled successful visualization of the atomic distribution of Fe, showing individual Fe atoms dispersed in few-layer graphene sheet. In addition, the EELS spectra clearly confirmed the identity of the bright spots as Fe atoms, along with the presence of N atoms in close proximity. Despite the atomic resolution of EELS, it was challenging to determine the oxidation state of Fe because of the weak signal and instability of Fe atoms under the electron beam. Similar to XAS analysis, such high-resolution STEM images couple with EELS at the atomic level have become the standard characterization to study single metal site catalysts.

4.4. Active site quantification in single metal site electrocatalysts

Along with identifying atomic configuration of single metal sites in catalysts using XAS, XPS, and STEM, quantifying catalytic active site concentrations/amounts are also of importance for evaluating intrinsic catalytic activities, understanding catalytic mechanisms, and rational design of novel single metal site electrocatalysts. Atomic concentration of a single metal site electrocatalysts can be determined using XPS or inductively coupled plasma atomic emission spectroscopy (ICP-AES) [121]; however, it is hard to deduce that all the single-atoms are at the surface and participating in electrochemical reactions. To quantify actual active sites in catalysts, ^{57}Fe Mössbauer spectroscopy and chemisorption-desorption methods have been developed. As shown in Figure 6C and D, two different types of atomic configuration of FeN_4 active sites (D1 and D2)

derived from Fe-doped ZIF-8 could be differentiated and quantified through the ^{57}Fe Mössbauer spectroscopy fitting[91]. Sahraie *et al*. quantified active sites of an Fe-N-C catalyst by using low temperature (193 K) CO pulse chemisorption and temperature-programmed desorption in a combination of Mössbauer spectroscopy [92]. From ^{57}Fe Mössbauer spectroscopy fitting, maximum mass-based site densities (MSD_{max}) was determined based on the amount of FeN_4 sites. Density of active sites (mass-based surface site density, MSD) were derived from the amount of adsorbed CO per $mg_{catalyst}$. The ratio of MSD/MSD_{max} was introduced as an active-site utilization factor, indicating a ratio of actually accessible sites for ORR over the total number of catalytically active sites. Malko *et al.* demonstrated a protocol to determine active site concentrations and determine the TOF of Fe-N-C catalysts by means of nitrite (NO_2^-) adsorption followed by reductive stripping [122]. The nitrite anion can strongly interact with the single Fe sits in catalysts. As a result, a stable poisoned catalyst adduct is formed. The adduct is stable enough while performing an ORR scan and it was found that ORR performance was degraded with nitrite adsorption. Under the appropriate condition of low potentials, reductive nitrate stripping occurred, and ORR catalytic activity was fully recovered. With the excess coulometric charge associated with the nitrate stripping, the number of active sites/ surface area as well as the number of active sites per mass were determined.

Additionally, inspiration can be drawn from methods to quantify active sites of thermochemical catalysts to develop routes of quantifying the density of active sites in catalysts. For example, active sites of isolated Rh on TiO_2 support for CO_2 reduction were quantified with diffuse reflectance infrared Fourier transform spectroscopy (DRIFTS) by comparing DRIFT spectra acquired before and after CO adsorption [95]. To quantify the density of active sites of Pt single atom catalysts for CO oxidation, Ding *et al*. [123]demonstrated infrared spectroscopy can

be a simple and convenient method. The band related to CO molecules adsorbed on Pt nanoparticles and Pt single atoms were assigned and the population of single-atom and nanoparticle was determined using temperature-programmed oxidation coupled with mass spectroscopy. From these data, they quantified CO adsorption sites both for single-atom and nanoparticle. It should be noted that, due to the heterogeneity of the active sites present in M-N-C catalysts, it is still difficult to conclusively quantify the number of surface accessible active sites and thereby calculating precise intrinsic activities. Improved techniques are also needed to provide versatility and specificity between different active site structures, including different transition metal identities.

4.5. *In situ* characterization

While *ex situ* characterization of catalysts by using microscopic and spectroscopic techniques has provided an unprecedented level of understanding of this important class of materials, the properties of the active single metal site either as prepared or post catalytic testing are not always reflective of the properties of these materials under operating conditions. Therefore, *in situ* or *operando* characterization is essential to understand the physical and chemical properties of these catalysts under electrochemical reaction conditions. This insight will enable scientists to advance their understanding of these catalyst materials and refine computational models to more accurately reflect catalyst structures under reaction conditions to gain improved insight into reaction mechanisms and structure-performance-property relationships.

In situ characterization has significantly advanced the scientific understanding of heterogeneous catalysts for thermochemical reactions [124], and these techniques should be exploited to advance our understanding of single metal site electrocatalysts under electrochemical reaction conditions, where challenges such as electrochemical reactor designs, and electrolyte attenuation of X-ray

signals are important challenges that must be addressed. Recently, *in situ* XANES has been applied to identify active site structures of single metal site electrocatalysts under reaction conditions. Fe K-edge XANES spectra were acquired for Fe-N-C ORR catalysts under different electrochemical potentials and in different O_2/N_2 saturated electrolyte environments [125]. It was found that a reduction of O_x-Fe^{3+}-N_4 to HO-*Fe^{2+}-N_4, which serve as an actual active site for the ORR at potentials below the Fe^{2+}/Fe^{3+} redox potential [58]. Ideally, multimodal *in situ* approaches can also be coupled together to provide a complete understanding of the structure-property-performance correlations of single metal site electrocatalysts.

5. Applications of single metal site electrocatalysts

Electrochemical energy conversion has long been deemed as integral components of a sustainable energy future. The practical implementation of these technologies, however, relies on the availability of active, selective, efficient, stable, and low cost electrocatalysts. Atomically dispersed supported single metal site electrocatalysts provide great potential to meet these rigorous requirements, and they have been extensively studied for a wide range of electrochemical energy conversion reactions. Here, progress made in the development of single metal site electrocatalysts for applications towards the ORR, OER, HER and CO_2RR will be discussed. Meanwhile, the in-depth understanding of catalytic performance enhancement mechanisms for both PGM and PGM-free site catalysts will be highlighted.

5.1 PGM site catalysts

Oxygen reduction reaction

ORR is the cathode reaction in fuel cells, normally undergoes a four electron ($4e^-$) pathways ($O_2 + 4H^+ + 4e^- \rightarrow 2H_2O$), during which O_2 adsorbs on the active sites and O-O bond were clipped for producing H_2O. The two-electron ($2e^-$) pathways ($O_2 + 2H^+ + 2e^- \rightarrow H_2O_2$) for the ORR is usually desired for electrochemical production of H_2O_2. For Pt nanoclusters and nanoparticles, which could provide two continued atoms for Pt-O-O-Pt adsorption, O-O bond would be easily clipped and ORR follows the $4e^-$ pathway. For ORR on isolated single Pt atoms, the electron transfer path would be varied depending on their support and coordination environment. An eye-catching phenomenon is that when Pt single atoms stabilized on *N*-vacancy of TiN and *C*-vacancy of TiC, the reaction path toward ORR was altered to $2e^-$ pathway due to that the metal-support interactions changed the adsorption energy toward O_2 and thus weakened the capability for scissoring the O-O bond [33]. The selectivity of Pt single atoms toward H_2O_2 production using TiN as support reached to 53.1%, and increased to 68% when the support was replaced by TiC due to the weaker affinity of oxygen species on these catalysts that preserved the O-O bond compared with that of TiN, as shown in **Figure 7**A [33]. The effects of carbon vacancies on the stabilization of single metal atoms (*i.e.* Au, Ag, Pd, Pt, Cu and Ni) was systematically investigated on TiC via experiments and DFT calculations, illuminating that their activity toward H_2O_2 selectivity follows the trend of Au>Pd>Ag>Cu>Pt based on calculated thermodynamic overpotentials [32]. Promising H_2O_2 selectivity of up to 92%-96% was delivered by chelating Pt single atoms with S atoms due to the strong Pt-S interaction on different types of support materials [126, 127]. Chelating with S induced the distortion of the Pt center off the square planar geometry (shown in Figure 7B) due to the more favorable interaction with water molecules. DFT calculation validated that the two electron pathway was kinetically favorable rather than thermodynamically favorable.

Pt single atoms immobilized on defect-enriched carbon materials, such as Pt single atoms bonded with pyridinic-N [128] or carbon divacancy (Pt-C_4 active sites) [129] preferentially displayed $4e^-$ ORR electrocatalysis. Theoretical calculations corroborated that nitrogen doping, especially pyridinic-N on carbon materials, could facilitate the accumulation of positive charges, leading to the up-shift of *d*-band centers toward Fermi level [129]. The positively charged active sites decreased the energy barrier for O_2 dissociation, thus favoring the 4e- pathways toward ORR. The Pt-N active sites anchored carbon cathode reported by Sun's research group yielded a maximum power density of 680 mW cm^{-2} at 80 ^oC in acidic single-cell with the noble metal utilization reached to 0.13 g_{Pt} KW^{-1} [128]. Other than Pt, Ir single atoms could also be grafted into carbon matrix for potential applications in electrocatalysis toward the ORR. Xiao et al., successfully impregnated Ir precursors into ZIF-8 via space confining effect [130]. This as-prepared Ir single atom-decorated catalysts exhibited the record-high TOF up to 24.3 e^{-1} $site^{-1}$ s^{-1}, far surpassing commercial Pt/C (3.63 e^{-1} $site^{-1}$ s^{-1}) and other ever-reported Pt-free ORR electrocatalysts. Although the promising catalytic activity was observed with the single Pt or Ir site catalysts, there stability was not discussed at all, which could be a serious issue for practical applications. In addition, increasing the loading of single metal sites in supported catalysts to meet the required performance metrics represents a grand challenge as well.

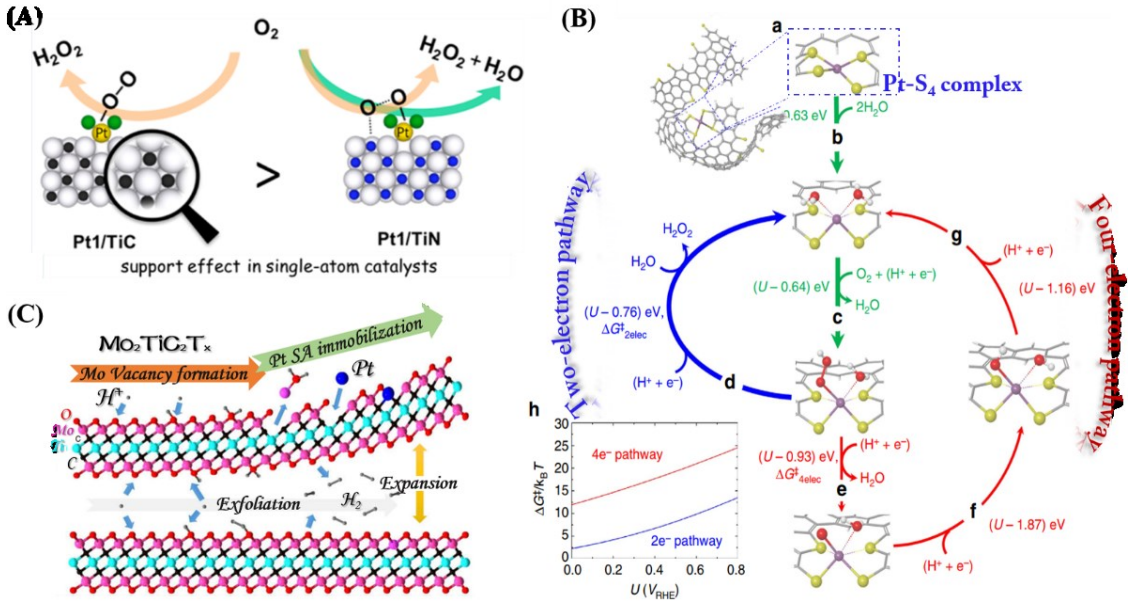

Figure 7. (A) Support effect in altering the reaction selectivity by Pt_1/TiN and Pt_1/TiC. Reproduced with permission from ref [33]. Copyright 2017, American Chemical Society. Pt-S_4 complex embedded in carbon support altered the reaction pathway favored by reaction kinetics. Reproduced with permission from ref [126]. Copyright 2016, Springer Nature. (C) Schematic illustration Pt Single atoms immobilized on Mo vacancies in *in situ* exfoliated 2D $Mo_2TiC_2T_x$ nanosheet. Reproduced with permission from ref [131]. Copyright 2018, Springer Nature.

The oxygen evolution and hydrogen evolution reactions for water electrolyzers

Electrochemical production of hydrogen fuel through water electrolysis is indispensable in realizing the application of renewable and environmental-benign energy conversion technologies. The OER is the reverse process of the ORR and is an important anode reaction in renewable energy conversion devices such as water electrolyzers, electrosynthesis, and metal-air batteries. Noble metal single atom-based catalysts for the OER have been rarely reported, especially in acidic electrolyte. Even though several works reported the atomically dispersed Ir species on $Co(OOH)_x$

nanosheet and Pt single atoms grafted on FeN_4 active sites applied for OER in alkaline medium, their catalytic performance is far from the best PGM-free electrocatalysts for the OER [103, 132, 133].

The cathode reaction of water electrolyzers is the HER for the production of hydrogen, ideally using renewable sources of electricity. The HER reaction path involves with either a Volmer-Tafel step or a Volmer-Heyrovsky step in acidic electrolyte, as shown in the following equations:

(Volmer) $H^+ + e^- = H_{ads}$ (1)

(Tafel) $H_{ads} + H_{ads} = H_2$ (2)

Or (Heyrovsky) $H_{ads} + H^+ + e^- = H_2$ (3)

Commercialized electrocatalysts for the HER are Pt/C. The scarcity of Pt expediated the HER catalyst engineering to reduce the loading of Pt or discovering alternative PGM-free catalysts. Due to the absence of ensemble sites, the HER catalysis path can be altered. For example, Pt single atoms on C-vacancies of TiC follows the Volmer-heyrovsky mechanism due to the lack of ensembles for enabling the traditional Volmer-Tafel mechanism [32]. HER catalytic activity of these transitional metal single atom incorporated catalysts followed the order of Pt > Ni > Pd > Au > Cu > Ag, and the enhanced performance correlated with their up-shifts of *d*-band center of Pt, Ni and Pd towards the Fermi level [32]. In addition to metal carbides, a variety of supported materials were also reported for anchoring Pt single atoms for HER electrocatalysis. Tavakkoli and co-workers successfully immobilized isolated Pt atoms onto single-walled carbon nanotubes with surface Pt loading as low as 0.19-0.75 at.% through electroplating deposition and attained the comparable catalytic activity with commercial Pt/C [134]. The interplay between the grafted individual Pt atoms and MoS_2 nanosheet for enhancing the HER catalysis were elucidated, stating that the enhanced catalysis behavior originated from the modulated adsorption energy toward H*

on adjacent S atom as a consequence of electronic reconfiguration of Pt-MoS_2 [34]. Mxenes, a new family of 2D materials, bearing the merits of plentiful exposed basal planes with outstanding metallic conductivity, high hydrophilicity and superior chemical stability, are postulated as feasible matrices for anchoring noble metal single atoms. For instance, Pt single atoms are successfully incorporated in Mo vacancies on the out-layer of Mxenes ($Mo_2TiC_2T_x$) as displayed in **Figure 7C** [131]. Inserted Pt single atoms improved the electronic conductivity of the matrix and favored the exceptional catalytic efficiency and stability toward HER.

5.2 PGM-free site catalysts

The oxygen reduction reaction for PEMFCs

Among studied PGM-free catalysts for the ORR, metal-nitrogen-carbon (M-N-C) materials (where M is commonly Fe, Co, Ni or Mn) have shown the most promise. The likely active sites in M-N-C catalysts are the carbon supported and nitrogen coordinated single metal sites, i.e. MN_4 moieties. Depending on the type of metals and local coordination environments, the intrinsic nature of adsorption energies toward O_2 and ability for breaking O-O bonding results in their different catalytic activities and stabilities [57, 135]. M-N-C electrocatalysts are generally synthesized by incorporating metal precursors into the nitrogen doped carbon precursors either by wet chemical adsorption process or by physical mix, and then subjected to high temperature pyrolysis. However, efficient M-N-C electrocatalysts are highly dependent on the properties of carbon matrix (nitrogen types and content, porosity, graphitization etc.), adsorption strategies, doping content, pyrolysis temperature and so on. Single Fe site-rich Fe-N-C catalysts have been the most extensively investigated owing to their intrinsically high catalytic activity in both acidic and alkaline electrolytes, in comparison to other M-N-C catalysts [18].

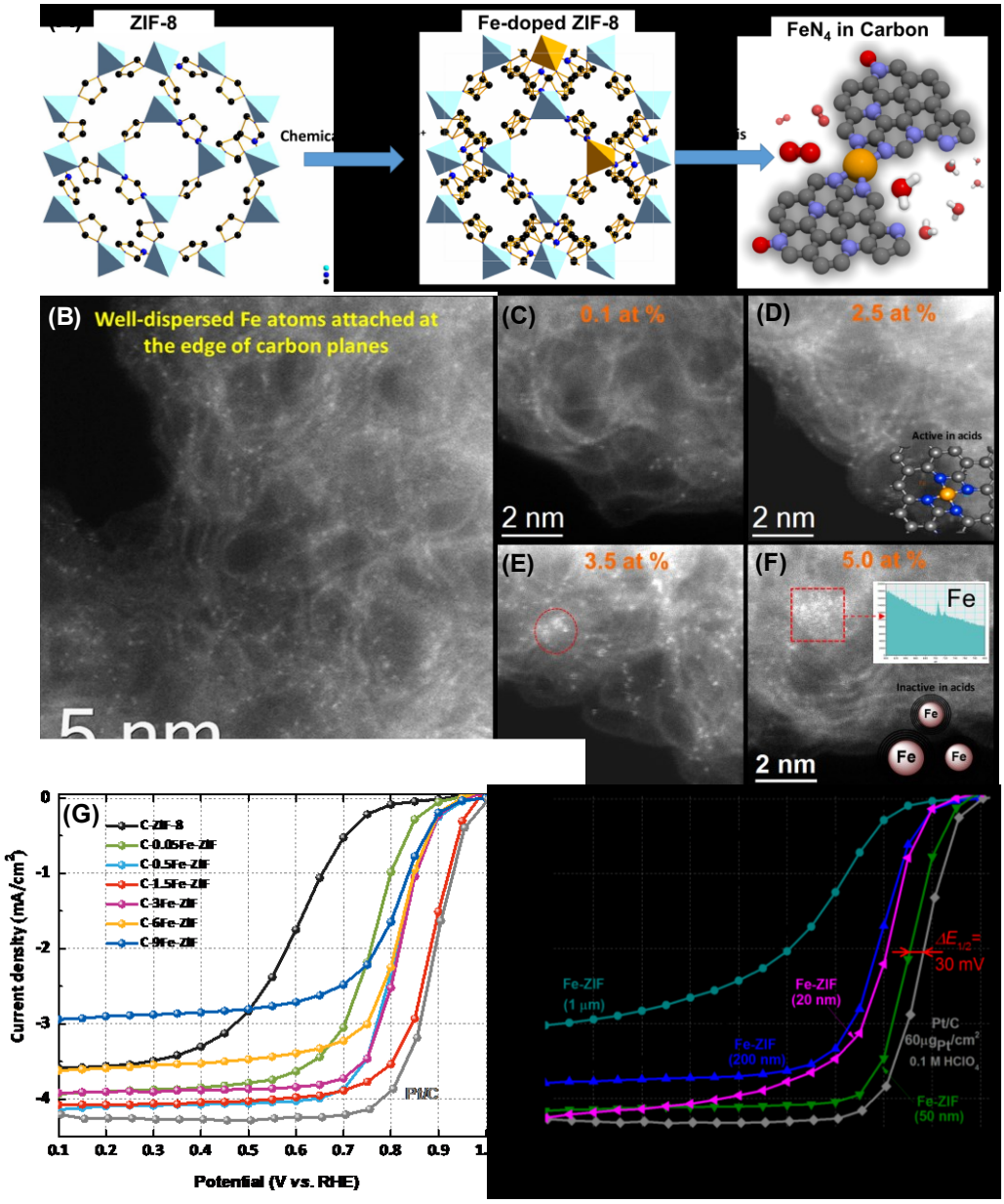

Figure 8. (A) Schematic illustration of the synthesis and TEM images of Fe-doped ZIF-8 polyhedral nanocrystals with different sizes; (B) STEM images showing complete single metal site distribution uniformly on partially graphitized carbon. (C-F) Transition of atomically dispersed single metal sites to metallic cluster with an increase of doping content of Fe during the

synthesis. Corresponding ORR activities on the atomically dispersed Fe-N-C catalysts with (G) different Fe content and (H) Fe particle sizes. Reproduced with permission from ref [23, 91]. Copyright 2017, American Chemical Society; Copyright 2019, The Royal Society of Chemistry.

The most promising Fe-N-C electrocatalysts exclusively containing single Fe sites for the ORR in challenging acidic electrolyte were achieved by *in situ* chemical doping of Fe^{3+} and forming covalent chemical bonding of $Fe\text{-}N_4$ into ZIF-8 precursors as shown in **Figure 8**A [23, 91]. The best performing catalyst obtained from optimal Fe doping achieved an $E_{1/2}$ of ca. 0.87±0.01 V *vs*. RHE in 0.5 M H_2SO_4 electrolyte, comparable to that of commercial Pt/C, which corresponds to the exclusively atomic dispersion of single iron sites into partially graphitized carbon, suggesting maximum density of active sites (**Figure 8B**). However, gradually increasing Fe doping content eventually leads to the formation of inactive metal nanoclusters and nanoparticles (**Figure 8C-F**), causing a decline of active site density and corresponding decreased activity (**Figure 8G**). These studies have shown the importance of heat treatment and Fe-doping content for modifying the pyridinic N content, porosity and graphitization degree of the catalysts for boosting their electrochemical performances toward ORR in acidic electrolyte. In addition, the particle size of the ZIF-8 polyhedral nanocrystals could be altered from 20 to 1000 nm by simply tuning metal concentrations during the synthesis. The catalytic activities were closely related to the surface area of Fe-doped ZIF-8 nanocrystals with different particle sizes. 50 nm Fe-ZIF-8 derived nanocrystal delivered the best ORR activity (**Figure 8H**). It is well known that the Fenton reaction catalyzed by Fe ions in Fe-N-C catalysts accelerates membrane/ionomer degradation and carbon corrosion due to the formation of free radical species [136]. These issues could be mitigated by either enhancing the graphitization degree of the carbon support (to improve resistivity to carbon

corrosion), replacing the Fe-N-C catalysts with Fe-free Co- or Mn-N-C catalysts (to minimize the Fenton reaction), or by modulating Fe-N-C catalysts to maximize selectivity towards the four-electron ORR to minimize the produced amount of H_2O_2.

In addition to generating more single metal active sites, reactant accessibility to interior active sites and favorable mass transport through engineering meso- and macro-sized pores [62, 137] are also crucial for catalytic performance. Significant efforts have been devoted to creating optimal porous structures for improving their fuel cell performances using a various methods, such as hard template (*e.g.*, ZnO, SiO_2, Fe_3O_4, etc.) [138-140], soft template (*e.g.*, surfactant, polystyrene sphere etc.) [141, 142], or template-free of gaseous ammonia treatment [143]. One important work involved the creation of hollow structured N-coordinated dual site FeCo/N-C electrocatalysts with excellent catalytic activity and stability toward ORR catalysis in acidic electrolyte [144]. A worth-mentioned advantageous feature of the M-N-C catalysts toward the ORR is their high resistance toward the methanol, ammonia, and other poisoning chemicals, which holds a promise for applications in direct methanol fuel cells and direct ammonia fuel cells [73, 145, 146]. Because methanol crossover from anode to cathode may poison and interfere with ORR catalysis on Pt-based cathode catalysts, M-N-C catalysts offer potential to mitigate this issue.

Despite significant advances in the development of atomically dispersed single metal site electrocatalysts for the ORR, stability remains a grand challenge especially in harsh acidic electrolytes [147]. Degradation of intrinsic activity of single metal site catalysts has been attributed to the possible demetallation and carbon oxidation during the ORR [22, 148]. Therefore, strengthening M-N bonding and providing robust carbon supports are straightforward solutions to address the stability issue [148, 149]. Detailed degradation mechanisms of single metal site electrocatalysts have been discussed in our recent reviews [8, 62, 147]

CO_2 conversion to CO

Electrochemical CO_2 reduction has attracted extensive attention given its potential for the direct conversion of CO_2 into sustainable carbon-based fuels and chemicals ideally using renewable electricity as the input energy source [150-155]. Nevertheless, the ultimate viability of this approach depends strongly on the development of optimal catalysts that have high activity and selectivity [156, 157]. Noble metal catalysts such as Au [158-162] and Ag [163, 164] have shown significant selectivity to reduce CO_2 to CO at low overpotentials; however, the high cost of these metals motivates the exploration of earth-abundant and inexpensive alternatives as a priority. To this end, molecular catalysts [165-168], MOFs [169], and immobilized porphyrins [170] have shown selectivity for CO_2 reduction into CO, which has motivated efforts into the exploration of atomically dispersed supported metal site catalysts.

In this regard, atomically dispersed supported single metal site electrocatalysts are structurally analogous to homogeneous organometallic compounds. They provide several advantages over their homogeneous counterparts, including the fact that they are immobilized so that catalyst recovery/regeneration is not required, and they are generally supported by high surface area conductive substrates (*i.e.*, carbon) so that electron transport and fabrication into electrode structures are more straightforward processes. Single metal site electrocatalysts also retain several of the advantages of their homogeneous counterparts, such as well-defined active site structures that can achieve high reaction selectivity, whereby materials such as carbon supported Ni-N-C active sites have been shown to reduce CO_2 into CO at low overpotentials with Faradaic efficiency (FE) greater than 95% [42, 171, 172].

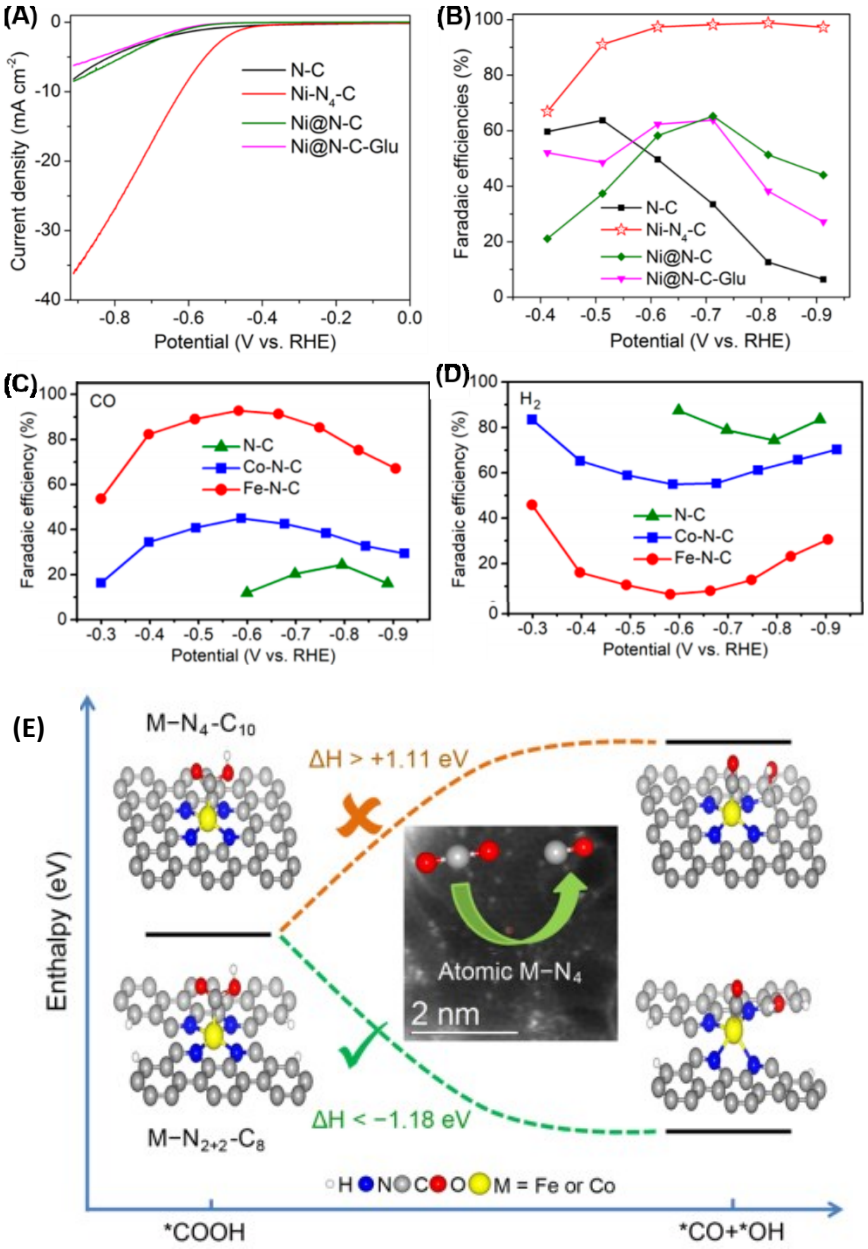

Figure 9. Electrochemical CO_2R (A) LSV curves and (B) FEs towards CO as a function of electrode potential for Ni-N-C based materials. Reproduced with permission from ref [42]. Copyright 2017, American Chemical Society. Electrochemical CO_2R FEs of M-N-C catalysts towards (C) CO and (D) H_2 at various electrode potentials. (E) DFT calculations on possible active

sites and reaction pathways. Reproduced with permission from ref [48]. Copyright 2018, American Chemical Society.

As expected, the type of transition metal center plays a significant impact on the properties and catalytic performance. Using a variety of metals including Co, Fe, Ni, Mn, and Cu, Ju et al., carried out a systematic investigation on N-coordinated single metal site carbon materials [173]. Significantly varying CO_2RR selectivity was observed for the different metal centers. Their obtained results showed that, for selective CO production, Ni-N-C and Fe-N-C catalysts are highly promising candidates [48, 172]. Interestingly, the Mn-N-C catalysts were also reported to electrochemically produce CH_4, albeit in very trace amounts. This early insight into the CO_2R activity and selectivity of M-N-C catalysts was leveraged to design Ni-N-C catalysts with very high (>90%) selectivity towards CO [111, 174-178]. Ni-N_4 site-rich catalysts were prepared by using a topo-chemical transformation strategy [42]. As exhibited in **Figure 9**A and **B**, high CO_2R FE of over 90% towards CO were observed in the electrode potential range from -0.5 to -0.9 V vs RHE, including a maximum FE of 99% and current density of 28.6 mA/cm^2 towards CO at an electrode potential of -0.81 V *vs*. RHE. Using a combination of XAS and HAADF-TEM, single metal sites, *i.e*. Ni-N_4 were verified dominant in these catalysts that provided excellent activity and selectivity towards CO, owing to favorable adsorption energies with reactive intermediates. This high selectivity of Ni-N-C catalysts towards CO is in good agreement with a study reported recently, showing 97% selectivity towards CO at an overpotential of 0.61 V [121]. Using operando XAS and XPS techniques, the presence of atomically dispersed Ni(I) sites was clearly identified, and that the high activity/selectivity arises due to the intrinsic activity of the Ni (I) metal sites. In addition, atomically dispersed single metal site-rich Fe-N-C catalysts for electrochemical CO_2RR

have also been extensively investigated [48, 173, 179-182]. Pan *et al*., elucidated the intrinsic activity and selectivity of well-defined atomically dispersed M-N_4 (M=Fe, Co) catalysts derived from chemically doped ZIF-8 precursors [48]. As shown in **Figure 9C** and **D**, the highest FEs reached to 93% towards CO was obtained by the Fe-N-C catalyst at an overpotential of 0.47 V, while the maximum FEs toward H_2 production is only 6% shown in Figure 9D, indicating that the HER was effectively suppressed on FeN_4 sites. Different from traditional MN_4C_{10} moieties in carbon plane as the active sites, the edge-hosted $MN_{2+2}C_8$ moieties bridging two armchair-like graphitic layers was postulated to be active moiety towards CO_2R based on the DFT calculations (**Figure 9E**).

The development of atomically dispersed and carbon supported M-N-C catalyst for electrochemical CO_2RR is rapidly evolving. A significant advantage of these materials is that they are commonly synthesized using simple methods and inexpensive precursors, rendering them as excellent candidate for manufacture scale up [183, 184]. Furthermore, the relatively high activity and selectivity that can be achieved on these materials for the conversion of CO_2 into CO have sparked significant research efforts on this topic. The formation of completely atomic dispersion of single metal sites in catalyst is very crucial for such high CO selectivity [171], instead of dominant H_2 evolution. Furthermore, any inadvertent contaminants such as unwanted transition metal aggregates (even in trace amounts) have been shown to dramatically impact experimentally measured electrochemical CO_2RR and H_2 evolution rates [185-187], so care must be taken when synthesizing and evaluating CO_2RR catalysts. Although such nitrogen-coordinated and carbon supported single metals site catalysts are incapable of directly reducing CO_2 to other more valuable C_2 products such as ethylene, they can be designed as a co-catalyst with others such as Cu for tandem conversion of CO_2 to CO and ethylene. Because Cu itself is not very active at producing

CO, an intermediate for ethylene production. Despite these challenges, very few studies have explored the co-catalyst approach with a certain degree of success [188-190].

6. Summary and outlook

Engineering highly efficient and inexpensive catalysts holds the key for expediting the development of sustainable energy conversion and storage technologies. On account of their unique quantum size effects, maximized metal atom utilization, and tunable metal-support interactions, atomically dispersed single metal site electrocatalysts have not only been investigated to advance fundamental scientific understanding of single atom chemistry, but have also emerged as a class of highly promising electrocatalyst for sustainable electrochemical energy conversion technologies. In this review, we first highlighted the fundamental basis for gaining understanding toward metal support interactions and probing the intrinsic active sites and origin of catalytic activities. Then, a brief introduction of the progress toward the synthesis strategies and characterization of single metal site electrocatalysts was provided, followed by the electrocatalysis applications towards various electrochemical reactions including ORR, OER, HER, and CO_2RR. While significant progress has been realized in synthesizing, characterizing and applying atomically dispersed supported single metal sites as electrocatalyst, there are several opportunities that still exist for advancing our scientific understanding and developing single metal site electrocatalysts with improved performance.

It is still elusive on the formation mechanism of single metal active sites, the origin of their activity as well as the structural evolution during the reactions. By virtue of the advanced characterization techniques and the DFT methods, fundamental understanding towards the role of single metal atoms in the reaction mechanisms is gaining clarity. Nevertheless, there still remains

some ambiguity, for example the formation mechanisms of MN_x moieties within carbon hosts, or the origin of ORR activity on CoN_x sites. In these cases, *in situ* characterization techniques along are required for monitoring the charge state variation or structural evolution under reaction conditions. This advanced understanding of single metal site properties will enable the establishment of structure-property-performance relationships that are reflective of the catalysts under reaction conditions. This scientific knowledge will provide more accurate input for computational simulations that can also incorporate machine learning algorithms for catalyst discovery [191, 192], and can also guide experimental catalyst design efforts where synthesis technique can be modified to target desirable catalyst properties.

It is still challenging to identify and quantify the exact number of available active sites present at the surface of catalysts. A large number of the single metal active site are likely buried in the interior (*i.e.*, bulk) of the catalysts and therefore not accessible to reactant species. Calculating turnover frequencies based on the total number of active sites in catalysts determined by using bulk techniques therefore leads to under-estimation of the intrinsic catalytic activities. Developing reliable means to quantify accessible surface residing active site structures can aid in achieving a quantitative evaluation and comparison of active site turnover frequencies, which will be crucial for achieving advanced fundamental insight into the performance of single metal site electrocatalysts. Furthermore, the effectiveness of developing synthesis strategies to maximize the accessibility of active site structures can also be effectively gauged if reliable methods for electrochemically accessible active site quantification exist.

Striking a delicate balance between catalytic activity and active site stability remains quite challenging, in that it has proven incredibly difficult to obtain electrocatalysts that display both excellent activity and stability. Regarding single metal site electrocatalysts, there are several

solutions for alleviating the stability issue, for instance, by selecting robust support materials with high corrosion- or oxidation-resistance abilities, or strengthening the metal-support interactions by choosing different nitrogen doping sources or varying the heating procedures.

Transferring catalytic performance measured in liquid electrolytes to more practical solid-state electrolyte, i.e. MEA remains a grand challenge. Constructing the relationship between their intrinsic activities/structures and their catalytic efficiencies are necessary for attaining a thorough comprehending toward engineering catalyst morphology and nanostructures with optimal porosity to increase accessible density of active sites and facilitate mass transport. For example, with an assistance of characterization techniques, structural evolution, active sites loss, charge and electronic conductivity variation during the long-term electrode/MEA operation would be monitored, affording valuable data for deducing their activity degradation mechanism, which in turn offers first-hand guidance for designing advanced performance catalysts designs.

The ability to leverage dual site catalysis, perhaps by having metal atoms side-by-side in the support materials is likely an effective strategy to design advanced electrocatalysts. This could provide opportunity to achieve the dissociative reduction of oxygen, or for promoting C-C coupling during the electrochemical CO_2 reduction to produce valuable C_2 chemicals such as ethanol or ethylene.

From a forward-looking perspective, the application of single metal site electrocatalysts is promising thanks to the development of synthesis strategies and encouraging electrocatalytic performances achieved recently. Additionally, opportunities exists to explore the possibility of preparing more types of catalysts active sites, for example, other metal single atoms that have not been extensively explored in the field of electrocatalysis, such as Cr, Mo, W, V, etc [193]. We believe that the continuous development of the mass-production of single metal site

electrocatalysts and the insightful fundamental understanding of the electrocatalysis mechanisms would propel their practical applications in electrochemical energy conversion technologies in the near future.

Acknowledgements

G.W. acknowledges the financial support from U.S. Department of Energy, Office of Energy Efficiency and Renewable Energy (EERE), Fuel Cell Technology Office (DE-EE0008075, DE-EE0008076, and DE-EE0008417) along with National Science Foundation (CBET-1604392, 1804326). D.H. acknowledges support from McMaster University and the National Science and Research Council of Canada (NSERC).

References

[1] H. Lv, D. Li, D. Strmcnik, A.P. Paulikas, N.M. Markovic, V.R. Stamenkovic, Nano Energy, 29 (2016) 149-165.

[2] Y. Zhu, J. Sokolowski, X. Song, Y. He, Y. Mei, G. Wu, Advanced Energy Materials, 10 (2019) 1902844.

[3] Q.R. Shi, Y. Cha, Y. Song, J.I. Lee, C.Z. Zhu, X.Y. Li, M.K. Song, D. Du, Y.H. Lin, Nanoscale, 8 (2016) 15414-15447.

[4] Q.R. Shi, S.F. Fu, C.Z. Zhu, J.H. Song, D. Du, Y. Lin, Materials Horizons, 6 (2019) 684-702.

[5] Q.R. Shi, C.Z. Zhu, D. Du, Y.H. Lin, Chemical Society Reviews, 48 (2019) 3181-3192.

[6] C.Z. Zhu, S.F. Fu, Q.R. Shi, D. Du, Y.H. Lin, Angewandte Chemie-International Edition, 56 (2017) 13944-13960.

[7] C.Z. Zhu, Q.R. Shi, S. Feng, D. Du, Y.H. Lin, Acs Energy Letters, 3 (2018) 1713-1721.

[8] X.X. Wang, M.T. Swihart, G. Wu, Nature Catalysis, 2 (2019) 578-589.

[9] Z. Chen, D. Higgins, A. Yu, L. Zhang, J. Zhang, Energy & Environmental Science, 4 (2011) 3167-3192.

[10] D.C. Higgins, Z. Chen, The Canadian Journal of Chemical Engineering, 91 (2013) 1881-1895.

[11] J. Liang, F. Ma, S. Hwang, X. Wang, J. Sokolowski, Q. Li, G. Wu, D. Su, Joule, 3 (2019) 956-991.

[12] X.X. Wang, S. Hwang, Y.-T. Pan, K. Chen, Y. He, S. Karakalos, H. Zhang, J.S. Spendelow, D. Su, G. Wu, Nano Letters, 18 (2018) 4163-4171.

[13] M. Chen, S. Hwang, J. Li, S. Karakalos, K. Chen, Y. He, S. Mukherjee, D. Su, G. Wu, Nanoscale, 10 (2018) 17318-17326.

[14] F. Jaouen, E. Proietti, M. Lefèvre, R. Chenitz, J.-P. Dodelet, G. Wu, H.T. Chung, C.M. Johnston, P. Zelenay, Energy & Environmental Science, 4 (2011) 114-130.

[15] G. Wu, Frontiers in Energy, 11 (2017) 286-298.

[16] Y. He, Q. Tan, L. Lu, J. Sokolowski, G. Wu, Electrochemical Energy Reviews, 2 (2019) 231-251.

[17] G. Wu, P. Zelenay, Accounts of Chemical Research, 46 (2013) 1878-1889.

[18] M. Chen, Y. He, J.S. Spendelow, G. Wu, Acs Energy Letters, 4 (2019) 1619-1633.

[19] X.J. Cui, W. Li, P. Ryabchuk, K. Junge, M. Beller, Nature Catalysis, 1 (2018) 385-397.

[20] J.Z. Li, M.J. Chen, D.A. Cullen, S. Hwang, M.Y. Wang, B.Y. Li, K.X. Liu, S. Karakalos, M. Lucero, H.G. Zhang, C. Lei, H. Xu, G.E. Sterbinsky, Z.X. Feng, D. Su, K.L. More, G.F. Wang, Z.B. Wang, G. Wu, Nature Catalysis, 1 (2018) 935-945.

[21] C.Z. Zhu, Q.R. Shi, B.Z. Xu, S.F. Fu, G. Wan, C. Yang, S.Y. Yao, J.H. Song, H. Zhou, D. Du, S.P. Beckman, D. Su, Y.H. Lin, Advanced Energy Materials, 8 (2018) 1801956.

[22] R. Chenitz, U.I. Kramm, M. Lefevre, V. Glibin, G.X. Zhang, S.H. Sun, J.P. Dodelet, Energy & Environmental Science, 11 (2018) 365-382.

[23] H.G. Zhang, S. Hwang, M.Y. Wang, Z.X. Feng, S. Karakalos, L.L. Luo, Z. Qiao, X.H. Xie, C.M. Wang, D. Su, Y.Y. Shao, G. Wu, Journal of the American Chemical Society, 139 (2017) 14143-14149.

[24] M. Hulsey, J.G. Zhang, N. Yan, Advanced Materials, 30 (2018) 1802304.

[25] S. Mukherjee, X. Yang, W. Shan, W. Samarakoon, S. Karakalos, D.A. Cullen, K. More, M. Wang, Z. Feng, G. Wang, G. Wu, Small Methods, 4 (2020) 1900821.

[26] K. Ithisuphalap, H. Zhang, L. Guo, Q. Yang, H. Yang, G. Wu, Small Methods, 3 (2019) 1800352.

[27] X.X. Wang, D.A. Cullen, Y.T. Pan, S. Hwang, M.Y. Wang, Z.X. Feng, J.Y. Wang, M.H. Engelhard, H.G. Zhang, Y.H. He, Y.Y. Shao, D. Su, K.L. More, J.S. Spendelow, G. Wu, Advanced Materials, 30 (2018) 1706758.

[28] Y. He, S. Hwang, D.A. Cullen, M.A. Uddin, L. Langhorst, B. Li, S. Karakalos, A.J. Kropf, E.C. Wegener, J. Sokolowski, M. Chen, D. Myers, D. Su, K.L. More, G. Wang, S. Litster, G. Wu, Energy & Environmental Science, 12 (2019) 250-260.

[29] Y. Hou, M. Qiu, M.G. Kim, P. Liu, G.T. Nam, T. Zhang, X.D. Zhuang, B. Yang, J. Cho, M.W. Chen, C. Yuan, L.C. Lei, X.L. Feng, Nature Communications, 10 (2019) 1392.

[30] H.L. Fei, J.C. Dong, Y.X. Feng, C.S. Allen, C.Z. Wan, B. Volosskiy, M.F. Li, Z.P. Zhao, Y.L. Wang, H.T. Sun, P.F. An, W.X. Chen, Z.Y. Guo, C. Lee, D.L. Chen, I. Shakir, M.J. Liu, T.D. Hu, Y.D. Li, A.I. Kirkland, X.F. Duan, Y. Huang, Nature Catalysis, 1 (2018) 63-72.

[31] Y. Zheng, Y. Jiao, Y.H. Zhu, Q.R. Cai, A. Vasileff, L.H. Li, Y. Han, Y. Chen, S.Z. Qiao, Journal of the American Chemical Society, 139 (2017) 3336-3339.

[32] S.K. Sahoo, Y. Ye, S. Lee, J. Park, H. Lee, J. Lee, J.W. Han, Acs Energy Letters, 4 (2019) 126-132.

[33] S. Yang, Y.J. Tak, J. Kim, A. Soon, H. Lee, Acs Catalysis, 7 (2017) 1301-1307.

[34] J. Deng, H.B. Li, J.P. Xiao, Y.C. Tu, D.H. Deng, H.X. Yang, H.F. Tian, J.Q. Li, P.J. Ren, X.H. Bao, Energy & Environmental Science, 8 (2015) 1594-1601.

[35] J. Yang, B.X. Chen, X.K. Liu, W. Liu, Z.J. Li, J.C. Dong, W.X. Chen, W.S. Yan, T. Yao, X.Z. Duan, Y. Wu, Y.D. Li, Angewandte Chemie-International Edition, 57 (2018) 9495-9500.

[36] Y.T. Qu, B.X. Chen, Z.J. Li, X.Z. Duan, L.G. Wang, Y. Lin, T.W. Yuan, F.Y. Zhou, Y.D. Hu, Z.K. Yang, C.M. Zhao, J. Wang, C. Zhao, Y.M. Hu, G. Wu, Q.H. Zhang, Q. Xu, B.Y. Liu, P. Gao, R. You, W.X. Huang, L.R. Zheng, L. Gu, Y. Wu, Y.D. Li, Journal of the American Chemical Society, 141 (2019) 4505-4509.

[37] L. Zhao, Y. Zhang, L.B. Huang, X.Z. Liu, Q.H. Zhang, C. He, Z.Y. Wu, L.J. Zhang, J.P. Wu, W.L. Yang, L. Gu, J.S. Hu, L.J. Wan, Nature Communications, 10 (2019) 1278.

[38] S. Gupta, S. Zhao, O. Ogoke, Y. Lin, H. Xu, G. Wu, ChemSusChem, 10 (2017) 774-785.

[39] Z. Qiao, H. Zhang, S. Karakalos, S. Hwang, J. Xue, M. Chen, D. Su, G. Wu, Applied Catalysis B: Environmental, 219 (2017) 629-639.

[40] M.C. Biesinger, B.P. Payne, L.W.M. Lau, A. Gerson, R.S.C. Smart, Surface and Interface Analysis, 41 (2009) 324-332.

[41] D.C. Koningsberger, Prins, R., Wiley, (1988).

[42] J.Y. Liu, Acs Catalysis, 7 (2017) 34-59.

[43] S. Mukerjee, S. Srinivasan, M.P. Soriaga, J. Mcbreen, Journal of the Electrochemical Society, 142 (1995) 1409-1422.

[44] Y. Peng, B.Z. Lu, S.W. Chen, Advanced Materials, 30 (2018) 1801995.

[45] Z.W. Chen, L.X. Chen, C.C. Yang, Q. Jiang, Journal of Materials Chemistry A, 7 (2019) 3492-3515.

[46] H.X. Xu, D.J. Cheng, D.P. Cao, X.C. Zeng, Nature Catalysis, 1 (2018) 339-348.

[47] K.X. Liu, Z. Qiao, S. Hwang, Z.Y. Liu, H.G. Zhang, D. Su, H. Xu, G. Wu, G.F. Wang, Applied Catalysis B-Environmental, 243 (2019) 195-203.

[48] F.P. Pan, H.G. Zhang, K.X. Liu, D. Cullen, K. More, M.Y. Wang, Z.X. Feng, G.F. Wang, G. Wu, Y. Li, Acs Catalysis, 8 (2018) 3116-3122.

[49] K. Liu, G. Wu, G. Wang, The Journal of Physical Chemistry C, 121 (2017) 11319-11324.

[50] X.F. Yang, A.Q. Wang, B.T. Qiao, J. Li, J.Y. Liu, T. Zhang, Accounts of Chemical Research, 46 (2013) 1740-1748.

[51] L. Nie, D.H. Mei, H.F. Xiong, B. Peng, Z.B. Ren, X.I.P. Hernandez, A. DeLariva, M. Wang, M.H. Engelhard, L. Kovarik, A.K. Datye, Y. Wang, Science, 358 (2017) 1419-+.

[52] J.W. Wan, W.X. Chen, C.Y. Jia, L.R. Zheng, J.C. Dong, X.S. Zheng, Y. Wang, W.S. Yan, C. Chen, Q. Peng, D.S. Wang, Y.D. Li, Advanced Materials, 30 (2018) 1705369.

[53] B.T. Qiao, J.X. Liang, A.Q. Wang, C.Q. Xu, J. Li, T. Zhang, J.Y. Liu, Nano Research, 8 (2015) 2913-2924.

[54] B.T. Qiao, A.Q. Wang, X.F. Yang, L.F. Allard, Z. Jiang, Y.T. Cui, J.Y. Liu, J. Li, T. Zhang, Nature Chemistry, 3 (2011) 634-641.

[55] A. Bruix, Y. Lykhach, I. Matolinova, A. Neitzel, T. Skala, N. Tsud, M. Vorokhta, V. Stetsovych, K. Sevcikova, J. Myslivecek, R. Fiala, M. Vaclavu, K.C. Prince, S. Bruyere, V.

Potin, F. Illas, V. Matolin, J. Libuda, K.M. Neyman, Angewandte Chemie-International Edition, 53 (2014) 10525-10530.

[56] K. Jiang, H.T. Wang, Chem, 4 (2018) 194-195.

[57] A. Zitolo, V. Goellner, V. Armel, M.T. Sougrati, T. Mineva, L. Stievano, E. Fonda, F. Jaouen, Nature Materials, 14 (2015) 937-+.

[58] M.L. Xiao, J.B. Zhu, L. Ma, Z. Jin, J. Ge, X.J. Deng, Y. Hou, Q.G. He, J.K. Li, Q.Y. Jia, S. Mukerjee, R. Yang, Z. Jiang, D.S. Su, C.P. Liu, W. Xing, Acs Catalysis, 8 (2018) 2824-2832.

[59] G. Wu, A. Santandreu, W. Kellogg, S. Gupta, O. Ogoke, H.G. Zhang, H.L. Wang, L.M. Dai, Nano Energy, 29 (2016) 83-110.

[60] Q. Jia, N. Ramaswamy, H. Hafiz, U. Tylus, K. Strickland, G. Wu, B. Barbiellini, A. Bansil, E.F. Holby, P. Zelenay, S. Mukerjee, Acs Nano, 9 (2015) 12496-12505.

[61] A. Zitolo, N. Ranjbar-Sahraie, T. Mineva, J.K. Li, Q.Y. Jia, S. Stamatin, G.F. Harrington, S.M. Lyth, P. Krtil, S. Mukerjee, E. Fonda, F. Jaouen, Nature Communications, 8 (2017) 957.

[62] X.X. Wang, Prabhakaran, V., He, Y. H., Shao, Y. Y., Wu, G., Advanced Materials, 31 (2019) 1805126.

[63] J. Wang, X.M. Ge, Z.L. Liu, L. Thia, Y. Yan, W. Xiao, X. Wang, Journal of the American Chemical Society, 139 (2017) 1878-1884.

[64] Y.H. He, S. Hwang, D.A. Cullen, M.A. Uddin, L. Langhorst, B.Y. Li, S. Karakalos, A.J. Kropf, E.C. Wegener, J. Sokolowski, M.J. Chen, D. Myers, D. Su, K.L. More, G.F. Wang, S. Litster, G. Wu, Energy & Environmental Science, 12 (2019) 250-260.

[65] H.G. Zhang, Chung, H. T., Cullen, D. A., Wagner, S., Kramm, U. I., More, K. L., Zelenay, P., Wu, G., Energy & Environmental Science, (2019).

[66] L. Jiao, Jiang, H. L. , Chem, 5 (2019) 1-19.

[67] S. Mukherjee, D.A. Cullen, S. Karakalos, K. Liu, H. Zhang, S. Zhao, H. Xu, K.L. More, G. Wang, G. Wu, Nano Energy, 48 (2018) 217-226.

[68] H. Zhang, H. Osgood, X. Xie, Y. Shao, G. Wu, Nano Energy, 31 (2017) 331-350.

[69] X. Wang, H. Zhang, H. Lin, S. Gupta, C. Wang, Z. Tao, H. Fu, T. Wang, J. Zheng, G. Wu, X. Li, Nano Energy, 25 (2016) 110-119.

[70] S.F. Ji, Y.J. Chen, S. Zhao, W.X. Chen, L.J. Shi, Y. Wang, J.C. Dong, Z. Li, F.W. Li, C. Chen, Q. Peng, J. Li, D.S. Wang, Y.D. Li, Angewandte Chemie-International Edition, 58 (2019) 4271-4275.

[71] S.F. Fu, C.Z. Zhu, D. Su, J.H. Song, S.Y. Yao, S. Feng, M.H. Engelhard, D. Du, Y.H. Lin, Small, 14 (2018).

[72] Y.Z. Chen, C.M. Wang, Z.Y. Wu, Y.J. Xiong, Q. Xu, S.H. Yu, H.L. Jiang, Advanced Materials, 27 (2015) 5010-5016.

[73] P.Q. Yin, T. Yao, Y. Wu, L.R. Zheng, Y. Lin, W. Liu, H.X. Ju, J.F. Zhu, X. Hong, Z.X. Deng, G. Zhou, S.Q. Wei, Y.D. Li, Angewandte Chemie-International Edition, 55 (2016) 10800-10805.

[74] Y.T. Qu, Z.J. Li, W.X. Chen, Y. Lin, T.W. Yuan, Z.K. Yang, C.M. Zhao, J. Wang, C. Zhao, X. Wang, F.Y. Zhou, Z.B. Zhuang, Y. Wu, Y.D. Li, Nature Catalysis, 1 (2018) 781-786.

[75] W.X. Chen, J.J. Pei, C.T. He, J.W. Wan, H.L. Ren, Y. Wang, J.C. Dong, K.L. Wu, W.C. Cheong, J.J. Mao, X.S. Zheng, W.S. Yan, Z.B. Zhuang, C. Chen, Q. Peng, D.S. Wang, Y.D. Li, Advanced Materials, 30 (2018) 1800396.

[76] W.X. Chen, J.J. Pei, C.T. He, J.W. Wan, H.L. Ren, Y.Q. Zhu, Y. Wang, J.C. Dong, S.B. Tian, W.C. Cheong, S.Q. Lu, L.R. Zheng, X.S. Zheng, W.S. Yan, Z.B. Zhuang, C. Chen, Q.

Peng, D.S. Wang, Y.D. Li, Angewandte Chemie-International Edition, 56 (2017) 16086-16090.

[77] Y. Yang, K.T. Mao, S.Q. Gao, H. Huang, G.L. Xia, Z.Y. Lin, P. Jiang, C.L. Wang, H. Wang, Q.W. Chen, Advanced Materials, 30 (2018) 1801732.

[78] B. Bayatsarmadi, Y. Zheng, A. Vasileff, S.Z. Qiao, Small, 13 (2017) 1700191.

[79] N. Ramaswamy, U. Tylus, Q.Y. Jia, S. Mukerjee, Journal of the American Chemical Society, 135 (2013) 15443-15449.

[80] W.J. Jiang, L. Gu, L. Li, Y. Zhang, X. Zhang, L.J. Zhang, J.Q. Wang, J.S. Hu, Z.D. Wei, L.J. Wan, Journal of the American Chemical Society, 138 (2016) 3570-3578.

[81] W. Wang, Q.Y. Jia, S. Mukerjee, S.L. Chen, Acs Catalysis, 9 (2019) 10126-10141.

[82] Q.H. Li, W.X. Chen, H. Xiao, Y. Gong, Z. Li, L.R. Zheng, X.S. Zheng, W.S. Yan, W.C. Cheong, R.A. Shen, N.H. Fu, L. Gu, Z.B. Zhuang, C. Chen, D.S. Wang, Q. Peng, J. Li, Y.D. Li, Advanced Materials, 30 (2018) 1800588.

[83] P.Z. Chen, T.P. Zhou, L.L. Xing, K. Xu, Y. Tong, H. Xie, L.D. Zhang, W.S. Yan, W.S. Chu, C.Z. Wu, Y. Xie, Angewandte Chemie-International Edition, 56 (2017) 610-614.

[84] Q. Li, G. Wu, D.A. Cullen, K.L. More, N.H. Mack, H.T. Chung, P. Zelenay, Acs Catalysis, 4 (2014) 3193-3200.

[85] G. Wu, C.M. Johnston, N.H. Mack, K. Artyushkova, M. Ferrandon, M. Nelson, J.S. Lezama-Pacheco, S.D. Conradson, K.L. More, D.J. Myers, P. Zelenay, Journal of Materials Chemistry, 21 (2011) 11392-11405.

[86] F. Pan, B. Li, E. Sarnello, S. Hwang, Y. Gang, X. Feng, X. Xiang, N.M. Adli, T. Li, D. Su, G. Wu, G. Wang, Y. Li, Nano Energy, (2019) 104384.

[87] C.Y. Ling, L. Shi, Y.X. Ouyang, X.C. Zeng, J.L. Wang, Nano Letters, 17 (2017) 5133-5139.

[88] U.I. Kramm, J. Herranz, N. Larouche, T.M. Arruda, M. Lefevre, F. Jaouen, P. Bogdanoff, S. Fiechter, I. Abs-Wurmbach, S. Mukerjee, J.P. Dodelet, Physical Chemistry Chemical Physics, 14 (2012) 11673-11688.

[89] Y. Mun, S. Lee, K. Kim, S. Kim, S. Lee, J.W. Han, J. Lee, Journal of the American Chemical Society, 141 (2019) 6254-6262.

[90] J.C. Li, X.P. Qin, P.X. Hou, M. Cheng, C. Shi, C. Liu, H.M. Cheng, M.H. Shao, Carbon, 147 (2019) 303-311.

[91] H.G. Zhang, H.T. Chung, D.A. Cullen, S. Wagner, U.I. Kramm, K.L. More, P. Zelenay, G. Wu, Energy & Environmental Science, 12 (2019) 2548-2558.

[92] N.R. Sahraie, U.I. Kramm, J. Steinberg, Y.J. Zhang, A. Thomas, T. Reier, J.P. Paraknowitsch, P. Strasser, Nature Communications, 6 (2015) 8618.

[93] R.E. Palmer, S. Pratontep, H.G. Boyen, Nature Materials, 2 (2003) 443-448.

[94] S. Dou, C.L. Dong, Z. Hu, Y.C. Huang, J.L. Chen, L. Tao, D.F. Yan, D.W. Chen, S.H. Shen, S.L. Chou, S.Y. Wang, Advanced Functional Materials, 27 (2017) 1702546.

[95] J.C. Matsubu, V.N. Yang, P. Christopher, Journal of the American Chemical Society, 137 (2015) 3076-3084.

[96] N.C. Cheng, S. Stambula, D. Wang, M.N. Banis, J. Liu, A. Riese, B.W. Xiao, R.Y. Li, T.K. Sham, L.M. Liu, G.A. Botton, X.L. Sun, Nature Communications, 7 (2016) 13638.

[97] L.J. Jingkun Li, Evan Wegener, Lynne Larochelle Richard, Ershuai Liu, Andrea Zitolo, Moulay Tahar Sougrati, Sanjeev Mukerjee, Zipeng Zhao, Yu Huang, Fan Yang, Sichen Zhong, Hui Xu,, F.r.J. A. Jeremy Kropf, Deborah J. Myers, and Qingying Jia, Journal of the American Chemical Society, (2019).

[98] J.Z. Li, H.G. Zhang, W. Samarakoon, W.T. Shan, D.A. Cullen, S. Karakalos, M.J. Chen, D.M. Gu, K.L. More, G.F. Wang, Z.X. Feng, Z.B. Wang, G. Wu, Angewandte Chemie-International Edition, (2019).

[99] Y. Cheng, S.Y. Zhao, B. Johannessen, J.P. Veder, M. Saunders, M.R. Rowles, M. Cheng, C. Liu, M.F. Chisholm, R. De Marco, H.M. Cheng, S.Z. Yang, S.P. Jiang, Advanced Materials, 30 (2018) 1706287.

[100] G. Wan, X.M. Lin, J.G. Wen, W.P. Zhao, L.Y. Pan, J. Tian, T. Li, H.R. Chen, J.L. Shi, Chemistry of Materials, 30 (2018) 7494-7502.

[101] J.D. Yi, R. Xu, Q. Wu, T. Zhang, K.T. Zang, J. Luo, Y.L. Liang, Y.B. Huang, R. Cao, Acs Energy Letters, 3 (2018) 883-889.

[102] B.W. Wang, X.X. Wang, J.X. Zou, Y.C. Yan, S.H. Xie, G.Z. Hu, Y.G. Li, A.G. Dong, Nano Letters, 17 (2017) 2003-2009.

[103] X.J. Zeng, J.L. Shui, X.F. Liu, Q.T. Liu, Y.C. Li, J.X. Shang, L.R. Zheng, R.H. Yu, Advanced Energy Materials, 8 (2018) 1701345.

[104] J.C. Li, Xiao, F., Zhong, H., Li, T., Xu, M. J., Ma, L., Cheng, M., Liu, D., Feng, S., Shi, Q. R., Cheng, H. M., Liu, C., Du, D., Beckman, S. P., Pan, X. Q., Lin, Y. H., Shao, M. H., ACS Catalysis, 9 (2019) 5929-5934.

[105] J.C. Li, Z.Q. Yang, D.M. Tang, L. Zhang, P.X. Hou, S.Y. Zhao, C. Liu, M. Cheng, G.X. Li, F. Zhang, H.M. Cheng, Npg Asia Materials, 10 (2018).

[106] Y.B. Yan, J.W. Miao, Z.H. Yang, F.X. Xiao, H.B. Yang, B. Liu, Y.H. Yang, Chemical Society Reviews, 44 (2015) 3295-3346.

[107] J. Jones, H.F. Xiong, A.T. Delariva, E.J. Peterson, H. Pham, S.R. Challa, G.S. Qi, S. Oh, M.H. Wiebenga, X.I.P. Hernandez, Y. Wang, A.K. Datye, Science, 353 (2016) 150-154.

[108] Z.P. Miao, X.M. Wang, M.C. Tsai, Q.Q. Jin, J.S. Liang, F. Ma, T.Y. Wang, S.J. Zheng, B.J. Hwang, Y.H. Huang, S.J. Guo, Q. Li, Advanced Energy Materials, 8 (2018) 1801226.

[109] Z.K. Yang, C.Z. Yuan, A.W. Xu, Acs Energy Letters, 3 (2018) 2383-2389.

[110] X.G. Li, W.T. Bi, L. Zhang, S. Tao, W.S. Chu, Q. Zhang, Y. Luo, C.Z. Wu, Y. Xie, Advanced Materials, 28 (2016) 2427-2431.

[111] K. Jiang, S. Siahrostami, T.T. Zheng, Y.F. Hu, S. Hwang, E. Stavitski, Y.D. Peng, J. Dynes, M. Gangisetty, D. Su, K. Attenkofer, H.T. Wang, Energy & Environmental Science, 11 (2018) 893-903.

[112] X.H. Huang, H. Yan, L. Huang, X.H. Zhang, Y. Lin, J.J. Li, Y.J. Xia, Y.F. Ma, Z.H. Sun, S.G. Wei, J.L. Lu, Journal of Physical Chemistry C, 123 (2019) 7922-7930.

[113] H.H. Wu, H.B. Li, X.F. Zhao, Q.F. Liu, J. Wang, J.P. Xiao, S.H. Xie, R. Si, F. Yang, S. Miao, X.G. Guo, G.X. Wang, X.H. Bao, Energy & Environmental Science, 9 (2016) 3736-3745.

[114] Y.T. Kim, K. Ohshima, K. Higashimine, T. Uruga, M. Takata, H. Suematsu, T. Mitani, Angewandte Chemie-International Edition, 45 (2006) 407-411.

[115] A.M. Venezia, Catalysis Today, 77 (2003) 359-370.

[116] G. Wu, D. Li, C. Dai, D. Wang, N. Li, Langmuir, 24 (2008) 3566-3575.

[117] G. Wu, M. Nelson, S. Ma, H. Meng, G. Cui, P.K. Shen, Carbon, 49 (2011) 3972-3982.

[118] G. Wu, R. Swaidan, D. Li, N. Li, Electrochimica Acta, 53 (2008) 7622-7629.

[119] H.T. Chung, D.A. Cullen, D. Higgins, B.T. Sneed, E.F. Holby, K.L. More, P. Zelenay, Science, 357 (2017) 479-483.

[120] P.F. Xie, T.C. Pu, A.M. Nie, S. Hwang, S.C. Purdy, W.J. Yu, D. Su, J.T. Miller, C. Wang, Acs Catalysis, 8 (2018) 4044-4048.

[121] H.B. Yang, S.F. Hung, S. Liu, K.D. Yuan, S. Miao, L.P. Zhang, X. Huang, H.Y. Wang, W.Z. Cai, R. Chen, J.J. Gao, X.F. Yang, W. Chen, Y.Q. Huang, H.M. Chen, C.M. Li, T. Zhang, B. Liu, Nature Energy, 3 (2018) 140-147.

[122] D. Malko, A. Kucernak, T. Lopes, Nature Communications, 7 (2016) 13285.

[123] K. Ding, A. Gulec, A.M. Johnson, N.M. Schweitzer, G.D. Stucky, L.D. Marks, P.C. Stair, Science, 350 (2015) 189-192.

[124] G. Malta, S.A. Kondrat, S.J. Freakley, C.J. Davies, L. Lu, S. Dawson, A. Thetford, E.K. Gibson, D.J. Morgan, W. Jones, P.P. Wells, P. Johnston, C.R.A. Catlow, C.J. Kiely, G.J. Hutchings, Science, 355 (2017) 1399-1402.

[125] Q.Y. Jia, N. Ramaswamy, U. Tylus, K. Strickland, J.K. Li, A. Serov, K. Artyushkova, P. Atanassov, J. Anibal, C. Gumeci, S.C. Barton, M.T. Sougrati, F. Jaouen, B. Halevi, S. Mukerjee, Nano Energy, 29 (2016) 65-82.

[126] C.H. Choi, M. Kim, H.C. Kwon, S.J. Cho, S. Yun, H.T. Kim, K.J.J. Mayrhofer, H. Kim, M. Choi, Nature Communications, 7 (2016) 10922.

[127] R.A. Shen, Chen, W. X., Peng, Q., Lu, S. Q., Zheng, L. R., Cao, X., Wang, Y., Zhu, Wei., Zhang, J. T., Zhuang, Z. B., Chen, C., Wang, D. S., Li, Y. D., Chem, (2019).

[128] J. Liu, M.G. Jiao, L.L. Lu, H.M. Barkholtz, Y.P. Li, Y. Wang, L.H. Jiang, Z.J. Wu, D.J. Liu, L. Zhuang, C. Ma, J. Zeng, B.S. Zhang, D.S. Su, P. Song, W. Xing, W.L. Xu, Y. Wang, Z. Jiang, G.Q. Sun, Nature Communications, 8 (2017) 15938.

[129] S.G. Liu, S.P. Huang, Carbon, 115 (2017) 11-17.

[130] M.L. Xiao, Zhu, J. B., Li, G. R., Li, N., Li, S., Cano, Z. P., Ma, L., Cui, P. X., Xu, P., Jiang, G. P., Jin, H. L., Wang, S., Wu, T. P., Lu, J., Yu, A. P., Su, D., Chen, Z. W., Angewandte Chemie-International Edition, 131 (2019) 9742-9747.

[131] J.Q. Zhang, Y.F. Zhao, X. Guo, C. Chen, C.L. Dong, R.S. Liu, C.P. Han, Y.D. Li, Y. Gogotsi, G.X. Wang, Nature Catalysis, 1 (2018) 985-992.

[132] L.Z. Zhang, Y. Jia, G.P. Gao, X.C. Yan, N. Chen, J. Chen, M.T. Soo, B. Wood, D.J. Yang, A.J. Du, X.D. Yao, Chem, 4 (2018) 285-297.

[133] S.F. Fu, J.H. Song, C.Z. Zhu, G.L. Xu, K. Amine, C.J. Sun, X.L. Li, M.H. Engelhard, D. Du, Y.H. Lin, Nano Energy, 44 (2018) 319-326.

[134] M. Tavakkoli, N. Holmberg, R. Kronberg, H. Jiang, J. Sainio, E.I. Kauppinen, T. Kallio, K. Laasonen, Acs Catalysis, 7 (2017) 3121-3130.

[135] G. Wu, K.L. More, C.M. Johnston, P. Zelenay, Science, 332 (2011) 443-447.

[136] C.H. Choi, C. Baldizzone, G. Polymeros, E. Pizzutilo, O. Kasian, A.K. Schuppert, N.R. Sahraie, M.T. Sougrati, K.J.J. Mayrhofer, F. Jaouen, ACS Catalysis, 6 (2016) 3136-3146.

[137] H.B. Tan, J. Tang, J. Kim, Y.V. Kaneti, Y.M. Kang, Y. Sugahara, Y. Yamauchi, Journal of Materials Chemistry A, 7 (2019) 1380-1393.

[138] H.W. Liang, W. Wei, Z.S. Wu, X.L. Feng, K. Mullen, Journal of the American Chemical Society, 135 (2013) 16002-16005.

[139] Z. Liu, F. Sun, L. Gu, G. Chen, T.T. Shang, J. Liu, Z.Y. Le, X.Y. Li, H.B. Wu, Y.F. Lu, Advanced Energy Materials, 7 (2017) 1701154.

[140] Z.L. Li, G.L. Li, L.H. Jiang, J.L. Li, G.Q. Sun, C.G. Xia, F.W. Li, Angewandte Chemie-International Edition, 54 (2015) 1494-1498.

[141] G. Lu, S.Z. Li, Z. Guo, O.K. Farha, B.G. Hauser, X.Y. Qi, Y. Wang, X. Wang, S.Y. Han, X.G. Liu, J.S. DuChene, H. Zhang, Q.C. Zhang, X.D. Chen, J. Ma, S.C.J. Loo, W.D. Wei, Y.H. Yang, J.T. Hupp, F.W. Huo, Nature Chemistry, 4 (2012) 310-316.

[142] K. Shen, L. Zhang, X.D. Chen, L.M. Liu, D.L. Zhang, Y. Han, J.Y. Chen, J.L. Long, R. Luque, Y.W. Li, B.L. Chen, Science, 359 (2018) 206-+.

[143] H.W. Liang, X.D. Zhuang, S. Bruller, X.L. Feng, K. Mullen, Nature Communications, 5 (2014).

[144] J. Wang, Z.Q. Huang, W. Liu, C.R. Chang, H.L. Tang, Z.J. Li, W.X. Chen, C.J. Jia, T. Yao, S.Q. Wei, Y. Wu, Y.D. Lie, Journal of the American Chemical Society, 139 (2017) 17281-17284.

[145] Z.X. Xia, Xu, X. L., Zhang, X. M., Li, H. Q., Wang, S. L., Sun, G. Q., Journal of Materials Chemistry A, 8 (2020) 1113-1119.

[146] N.M. Adli, H. Zhang, S. Mukherjee, G. Wu, Journal of the Electrochemical Society, 165 (2018) J3130-J3147.

[147] Y.Y. Shao, J.P. Dodelet, G. Wu, P. Zelenay, Advanced Materials, 31 (2019) 1807615.

[148] C.H. Choi, C. Baldizzone, J.P. Grote, A.K. Schuppert, F. Jaouen, K.J.J. Mayrhofer, Angewandte Chemie-International Edition, 54 (2015) 12753-12757.

[149] C.H. Choi, W.S. Choi, O. Kasian, A.K. Mechler, M.T. Sougrati, S. Bruller, K. Strickland, Q.Y. Jia, S. Mukerjee, K.J.J. Mayrhofer, F. Jaouen, Angewandte Chemie-International Edition, 56 (2017) 8809-8812.

[150] S. Lin, C.S. Diercks, Y.B. Zhang, N. Kornienko, E.M. Nichols, Y.B. Zhao, A.R. Paris, D. Kim, P. Yang, O.M. Yaghi, C.J. Chang, Science, 349 (2015) 1208-1213.

[151] N. Assen, Junga, J., Bardow, A., Energy & Environmental Science, 6 (2013) 2712-2734.

[152] P. De Luna, C. Hahn, D. Higgins, S.A. Jaffer, T.F. Jaramillo, E.H. Sargent, Science, 364 (2019) 350-+.

[153] D. Higgins, C. Hahn, C.X. Xiang, T.F. Jaramillo, A.Z. Weber, Acs Energy Letters, 4 (2019) 317-324.

[154] C. Long, X. Li, J. Guo, Y.N. Shi, S.Q. Liu, Z.Y. Tang, Small Methods, 3 (2019) 1800369.

[155] Y.L. Zheng, P. Cheng, J.S. Xu, J.Y. Han, D.W. Wang, C.L. Hao, H.R. Alanagh, C. Long, X.H. Shi, Z.Y. Tang, Nanoscale, 11 (2019) 4911-4917.

[156] H. Mistry, A.S. Varela, S. Kuhl, P. Strasser, B.R. Cuenya, Nature Reviews Materials, 1 (2016).

[157] B. Kumar, J.P. Brian, V. Atla, S. Kumari, K.A. Bertram, R.T. White, J.M. Spurgeon, Catalysis Today, 270 (2016) 19-30.

[158] Y. Hori, Modern Aspects of Electrochemistry, 42 (2008) 89-189.

[159] Y.H. Chen, C.W. Li, M.W. Kanan, Journal of the American Chemical Society, 134 (2012) 19969-19972.

[160] W.L. Zhu, R. Michalsky, O. Metin, H.F. Lv, S.J. Guo, C.J. Wright, X.L. Sun, A.A. Peterson, S.H. Sun, Journal of the American Chemical Society, 135 (2013) 16833-16836.

[161] W.L. Zhu, Y.J. Zhang, H.Y. Zhang, H.F. Lv, Q. Li, R. Michalsky, A.A. Peterson, S.H. Sun, Journal of the American Chemical Society, 136 (2014) 16132-16135.

[162] H. Mistry, R. Reske, Z.H. Zeng, Z.J. Zhao, J. Greeley, P. Strasser, B. Roldan Cuenya, Journal of the American Chemical Society, 136 (2014) 16473-16476.

[163] Q. Lu, J. Rosen, F. Jiao, Chemcatchem, 7 (2015) 38-47.

[164] H. Mistry, Y.W. Choi, A. Bagger, F. Scholten, C.S. Bonifacio, I. Sinev, N.J. Divins, I. Zegkinoglou, H.S. Jeon, K. Kisslinger, E.A. Stach, J.C. Yang, J. Rossmeisl, B. Roldan Cuenya, Angewandte Chemie-International Edition, 56 (2017) 11394-11398.

[165] M. Hammouche, D. Lexa, J.M. Saveant, M. Momenteau, Journal of Electroanalytical Chemistry, 249 (1988) 347-351.

[166] I. Bhugun, D. Lexa, J.M. Saveant, Journal of the American Chemical Society, 118 (1996) 1769-1776.

[167] Y. Hori, A. Murata, R. Takahashi, Journal of the Chemical Society-Faraday Transactions I, 85 (1989) 2309-2326.

[168] S.X. Ren, Joulié, D., Salvatore, D., Torbensen, K., Wang, M., Robert, M., Berlinguette, C. P. , Science, 365 (2019) 367-369.

[169] N. Kornienko, Y.B. Zhao, C.S. Kiley, C.H. Zhu, D. Kim, S. Lin, C.J. Chang, O.M. Yaghi, P.D. Yang, Journal of the American Chemical Society, 137 (2015) 14129-14135.

[170] A.S. Varela, N.R. Sahraie, J. Steinberg, W. Ju, H.S. Oh, P. Strasser, Angewandte Chemie-International Edition, 54 (2015) 10758-10762.

[171] D.M. Koshy, S.C. Chen, D.U. Lee, M.B. Stevens, A.M. Abdellah, S.M. Dull, G. Chen, D. Nordlund, A. Gallo, C. Hahn, D.C. Higgins, Z.N. Bao, T.F. Jaramillo, Angewandte Chemie-International Edition, (2020).

[172] F. Pan, H. Zhang, Z. Liu, D. Cullen, K. Liu, K. More, G. Wu, G. Wang, Y. Li, Journal of Materials Chemistry A, 7 (2019) 26231-26237.

[173] W. Ju, A. Bagger, G.P. Hao, A.S. Varela, I. Sinev, V. Bon, B. Roldan Cuenya, S. Kaskel, J. Rossmeisl, P. Strasser, Nature Communications, 8 (2017).

[174] T. Moller, W. Ju, A. Bagger, X.L. Wang, F. Luo, T.N. Thanh, A.S. Varela, J. Rossmeisl, P. Strasser, Energy & Environmental Science, 12 (2019) 640-647.

[175] K. Jiang, S. Siahrostami, A.J. Akey, Y.B. Li, Z.Y. Lu, J. Lattimer, Y.F. Hu, C. Stokes, M. Gangishetty, G.X. Chen, Y.W. Zhou, W. Hill, W.B. Cai, D. Bell, K.R. Chan, J.K. Norskov, Y. Cui, H.T. Wang, Chem, 3 (2017) 950-960.

[176] C.B. Lu, J. Yang, S. Wei, S. Bi, Y. Xia, M.X. Chen, Y. Hou, M. Qiu, C. Yuan, Y.Z. Su, F. Zhang, H.W. Liang, X.D. Zhuang, Advanced Functional Materials, 29 (2019) 1806884.

[177] P.L. Lu, Y.J. Yang, J.N. Yao, M. Wang, S. Dipazir, M.L. Yuan, J.X. Zhang, X. Wang, Z.J. Xie, G.J. Zhang, Applied Catalysis B-Environmental, 241 (2019) 113-119.

[178] P. Su, K. Iwase, S. Nakanishi, K. Hashimoto, K. Kamiya, Small, 12 (2016) 6083-6089.

[179] T.N. Huan, N. Ranjbar, G. Rousse, M. Sougrati, A. Zitolo, V. Mougel, F. Jaouen, M. Fontecave, ACS Catalysis, 7 (2017) 1520-1525.

[180] W.G. Liu, L.L. Zhang, X. Liu, X.Y. Liu, X.F. Yang, S. Miao, W.T. Wang, A.Q. Wang, T. Zhang, Journal of the American Chemical Society, 139 (2017) 10790-10798.

[181] A.S. Varela, M. Kroschel, N.D. Leonard, W. Ju, J. Steinberg, A. Bagger, J. Rossmeisl, P. Strasser, Acs Energy Letters, 3 (2018) 812-817.

[182] J. Gu, C.S. Hsu, L.C. Bai, H.M. Chen, X.L. Hu, Science, 364 (2019) 1091-1094.

[183] M. Lefevre, E. Proietti, F. Jaouen, J.P. Dodelet, Science, 324 (2009) 71-74.

[184] H.T. Chung, Johnston, C. M., Zelenay, P., ECS Trans., 25 (2009) 485-492.

[185] Y. Lum, Y. Kwon, P. Lobaccaro, L. Chen, E.L. Clark, A.T. Bell, J.W. Ager, ACS Catalysis, 6 (2016) 202-209.

[186] E.L. Clark, J. Resasco, A. Landers, J. Lin, L.T. Chung, A. Walton, C. Hahn, T.F. Jaramillo, A.T. Bell, ACS Catalysis, 8 (2018) 6560-6570.

[187] T. Wang, Q. Zhao, Y. Fu, C. Lei, B. Yang, Z. Li, L. Lei, G. Wu, Y. Hou, Small Methods, 3 (2019) 1900210.

[188] D. Choukroun, N. Daems, T. Kenis, T. Van Everbroeck, J. Hereijgers, T. Altantzis, S. Bals, P. Cool, T. Breugelmans, The Journal of Physical Chemistry C, 124 (2020) 1369-1381.

[189] T.T.H. Hoang, S. Verma, S. Ma, T.T. Fister, J. Timoshenko, A.I. Frenkel, P.J.A. Kenis, A.A. Gewirth, Journal of the American Chemical Society, 140 (2018) 5791-5797.

[190] D. Ren, B.S.-H. Ang, B.S. Yeo, ACS Catalysis, 6 (2016) 8239-8247.

[191] D.P. Tabor, L.M. Roch, S.K. Saikin, C. Kreisbeck, D. Sheberla, J.H. Montoya, S. Dwaraknath, M. Aykol, C. Ortiz, H. Tribukait, C. Amador-Bedolla, C.J. Brabec, B. Maruyama, K.A. Persson, A. Aspuru-Guzik, Nature Reviews Materials, 3 (2018) 5-20.

[192] S. Back, K. Tran, Z.W. Ulissi, ACS Catalysis, 9 (2019) 7651-7659.

[193] E.G. Luo, Zhang, H., Wang, X., Gao, L. Q., Gong, L. Y., Zhao, T., Jin, Z., Ge, J. J., Jiang, Z., Liu, C. P., Xing, W., Angewandte Chemie-International Edition, 58 (2019) 1-8.